# Online Oxide Contamination Measurement and Purification Demonstration

*D.E. Bradley*
*Yetispace, Inc., Huntsville, Alabama*

*T.J. Godfroy*
*Maximum Technology Corporation, Huntsville, Alabama*

*K.L. Webster, A.E. Garber, K.A. Polzin, and D.J. Childers*
*Marshall Space Flight Center, Huntsville, Alabama*

National Aeronautics and
Space Administration

Marshall Space Flight Center • Huntsville, Alabama  35812

# Acknowledgments

# TRADEMARKS

# TABLE OF CONTENTS

# LIST OF FIGURES

# LIST OF TABLES

# LIST OF ACRONYMS AND SYMBOLS

Ar          argon

CTMV        cold trap motor valve

Cu          copper

DAQ         data acquisition

DC          direct current

EFF-TF      Early Flight Fission Test Facility

EM          electromagnetic

EMF         electromagnetic force

FSP         fission surface power

FTL         feasibility test loop

GFSSP       Generalized Fluid System Simulation Program

$GN_2$      gaseous nitrogen

He          helium

HX          heat exchanger

ID          inside diameter

I/O         input/output

MSFC        Marshall Space Flight Center

MV          motor valve

NaK         sodium-potassium

O           oxygen

## LIST OF ACRONYMS AND SYMBOLS (Continued)

PMV  plugging motor valve

PT  pressure transducer

RT  real time

RTD  resistance temperature detector

SS  stainless steel

TC  thermocouple

TDU  Technology Demonstration Unit

TP  Technical Publication

# NOMENCLATURE

| | |
|---|---|
| $B$ | magnetic flux density (Tesla) |
| $\vec{E}$ | EMF generated |
| $K$ | constant |
| $l$ | length |
| $m$ | slope |
| $\dot{m}$ | mass flow rate |
| $s$ | height; ID of fluid-carrying conduit (cm) |
| $t$ | time |
| $u$ | volumetric flow rate |
| $u(t)$ | time-varying flow rate |
| $\dot{V}$ | volumetric flow of fluid (cc/s) |
| $v$ | signal voltage generated (mV) |
| $v(t)$ | time-varying voltage |
| $w$ | width |
| $\Delta P$ | change in pressure |
| $\rho$ | density |

TECHNICAL PUBLICATION


## ONLINE OXIDE CONTAMINATION MEASUREMENT AND PURIFICATION DEMONSTRATION


# 1.  INTRODUCTION


Fission surface power (FSP) systems could be used to provide power on the surface of the Moon, Mars, or other planets, asteroids, and moons of our solar system. In addition, fission power systems could provide excellent performance at any location, including heavily shaded or permanently shaded regions, and may offer the capability to provide on-demand power at any time, even at long distances from the Sun. Fission-based systems also offer the potential for outposts, crew, and science instruments to operate in a power-rich environment. NASA has been exploring technologies to reduce the cost and technical risk of employing FSP systems. A reference 40-kW$_e$ option has been devised that is cost competitive with alternatives while providing more power for less mass anywhere on the lunar surface. The reference FSP system is also readily extensible for use on Mars or virtually any other location in the solar system. On Mars, the system would be capable of operating through global dust storms and providing year-round power at any martian latitude.

The Early Flight Fission Test Facility (EFF-TF) at NASA Marshall Space Flight Center (MSFC) provides the capability to perform nonnuclear, hardware-based testing of concepts and components. Component design iterations benefit dramatically from low-cost, subscale testing. To this end, the FSP team has developed a feasibility test loop (FTL) that provides a subscale, high-temperature liquid metal flow loop for rapid, smaller scale component testing. This Technical Publication (TP) details continuous, long-term efforts to research, design, assemble, and test several subscale components—a mechanical coolant pump, a venturi flowmeter, electromagnetic (EM) flowmeters, oxide plugging indicator, and oxide removing cold trap—with the ultimate goal of showing flow loop contamination and purification via a plugging meter and cold trap.

## 1.1  Fission Surface Power Technology Development

Under the NASA Exploration Technology Development program, NASA and the Department of Energy have begun long-lead technology development for potentially supporting future integrated FSP systems. The major effort in the FSP technology project has been focused on a reference mission and concept. The reference mission is to provide electrical power to habitats anywhere on the lunar surface. The requirements derived from this mission are 40 kW$_e$ delivered to the habitat, and a design life of 8 yr. Although many options exist, NASA's current reference FSP system uses a fast spectrum, pumped liquid sodium-potassium- (NaK-) cooled reactor coupled to a Stirling power conversion subsystem. The reference system uses technology with significant terrestrial heritage that can operate at any location on the surface of the Moon, Mars, or elsewhere in the solar

system. Detailed development of the FSP concept and the reference mission are documented in various other reports.[1–4]

    The objectives of the FSP technology project are as follows:[5]

- Develop FSP concepts that meet expected surface power requirements at reasonable cost with added benefits over other options.

- Establish a nonnuclear, hardware-based technical foundation for FSP design concepts to reduce overall development risk.

- Reduce the cost uncertainties for FSP and establish greater credibility for flight system cost estimates.

- Generate key nonnuclear products to allow Agency decision makers to consider FSP as a viable option for potential future flight development.

    The current FSP concept draws heavily on existing component technologies to reduce cost and risk. The greatest technical challenge is to demonstrate that the components can function together as an integrated system. Making meaningful progress in FSP technology also requires hardware development and testing. In order to simultaneously pursue hardware advancement and address the concept's major technical challenge, the Technology Demonstration Unit (TDU) is currently under development. The TDU will contain a reactor simulator, power conversion unit, power management and distribution, two liquid metal pumps, and a heat rejection system. The TDU will address integrated system performance and control, liquid metal heat transport, electric power generation, and waste heat removal. It will not address issues involving the generation and control of nuclear heat, operational lifetime, and launch/landing survivability. During testing, the system will be subjected to realistic operating conditions; data will be gathered to better understand performance sensitivity, control sensitivity, and response characteristics. Upon completion of this testing, FSP will achieve a nonnuclear technology readiness level of 6: System Demonstration in an Operational Environment.

## 1.2 Nonnuclear Testing at Marshall Space Flight Center

    The EFF-TF was established by MSFC to perform hardware-directed activities to support multiple in-space nuclear reactor concepts by using a nonnuclear test methodology.[6–8] This includes fabrication and testing at both the module/component level and near prototypic reactor components and configurations, allowing for realistic thermal-hydraulic evaluations of systems. The FTL provides the means for evaluating preliminary component design and analysis in a hardware test bed. It uses pumped liquid metal NaK to simulate a primary reactor cooling system.

    For this test, the FTL employed an oxide measurement and purification system intended to demonstrate online coolant purification. A mechanical centrifugal pump provided NaK circulation. Electromagnetic flowmeters combined with a reference venturi flowmeter provided volumetric flow rate data. Calibration of EM flowmeters was performed in the past by an independent

contractor. The integration of a reference venturi flowmeter allowed in-loop calibration of EM flow-meters. Finally, a graphite resistance heater was installed to provide heat input to the system. This TP describes the design rationale, testing, and resulting performance characterization of the above components, as well as lessons learned in test that can be used for the benefit of the TDU.

## 2.  FEASIBILITY TEST LOOP OVERALL SYSTEM CONFIGURATION

While the overall objective of testing was to show contamination and purification in the FTL, several component iterations were devised and tested before the ultimate goal could be achieved. To that end, this configuration of the FTL served as a proof-of-concept testing platform for several new candidate component designs.

The test article consists of an all stainless steel (SS) primary flow loop using 0.5-in- (1.27-cm-) diameter tubing to connect the following major components: a graphite resistance heating element (heat input), a gaseous nitrogen ($GN_2$) counterflow heat exchanger (HX) (simulated heat load), a mechanical centrifugal NaK pump (coolant pump), direct current (DC) EM flowmeters and a venturi flowmeter (flow rate measurement), and a combined coolant contamination measuring/purification system. Figure 1 shows the major components of the FTL.
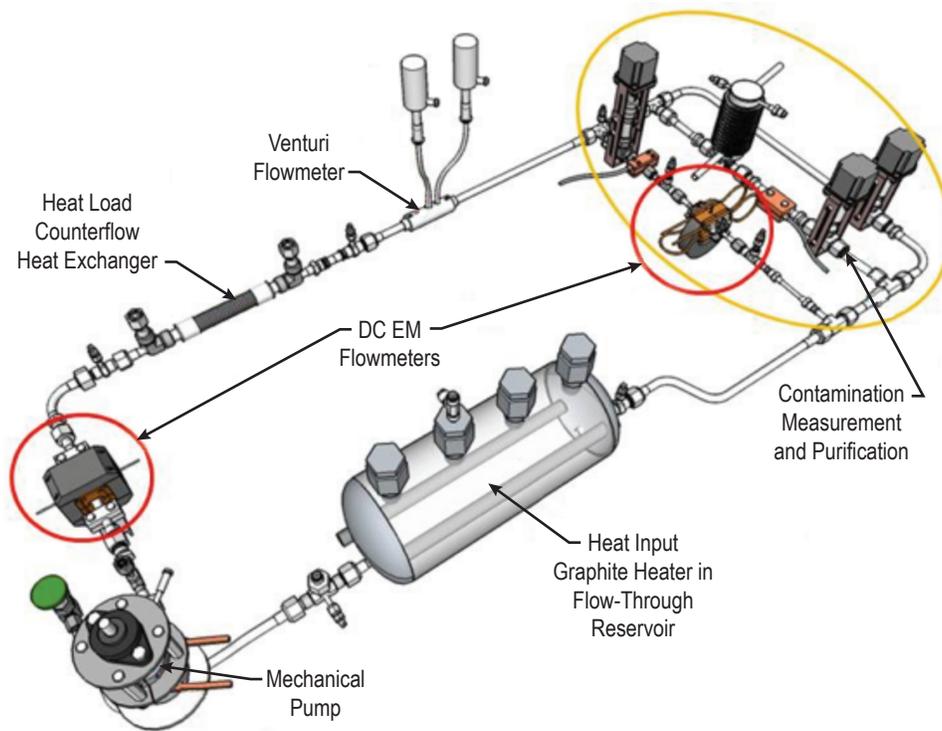


Figure 1.  Feasibility test loop overview.

In addition to the primary flow loop, the current configuration has two alternative, parallel flow branches available for conducting real-time NaK contamination measurement and purification. These branches are known as the plugging branch and the cold trap branch, and are user selectable via remotely operated motor-controlled valves. The primary loop is also provided with

a motor-operated valve so that any combination of flow through the three parallel branches is available during test. The parallel flow branches are highlighted in figure 2.
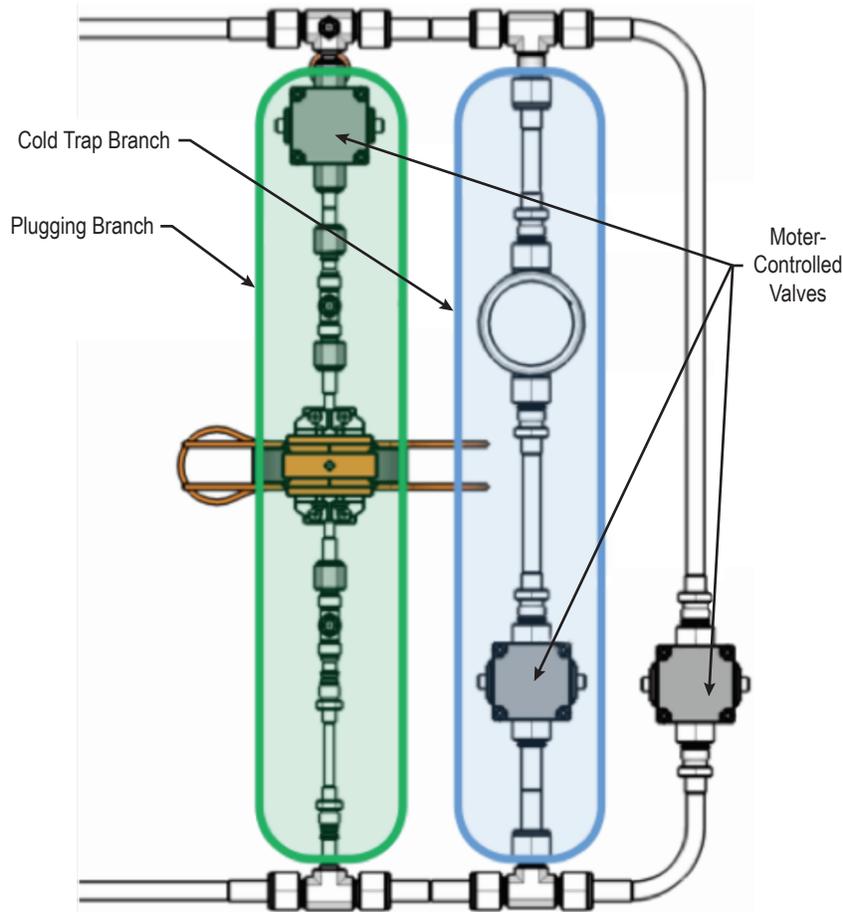


Figure 2.  Details of parallel flow branches.

## 2.1  Interfacing Systems

Since 2008 the FTL has been used to evaluate designs for EM flowmeters, plugging/oxide precipitation measurement devices, EM pumps, resistance and radio frequency heaters and bonded strain gauge pressure transducers. The results of these tests are documented in reference 8. The FTL is filled with the eutectic sodium-potassium alloy (NaK-78). NaK is liquid at room temperature even though sodium and potassium, as stand-alone elements, are solid at room temperature. NaK-78 has the lowest melting point of all NaK alloys. While NaK has excellent thermal conductivity properties, it is highly reactive in the presence of oxygen (O), particularly at elevated temperatures. For this reason, all testing of the apparatus is conducted within a 3-ft (~1-m) vacuum chamber. Vacuum levels reach the range of $10^{-3}$ torr. Should a leak develop while the FTL is hot, no O is present to burn. A second, equally important reason to operate under vacuum is to reduce thermal losses during hot tests. Figure 3 shows the test loop as installed inside the vacuum chamber.
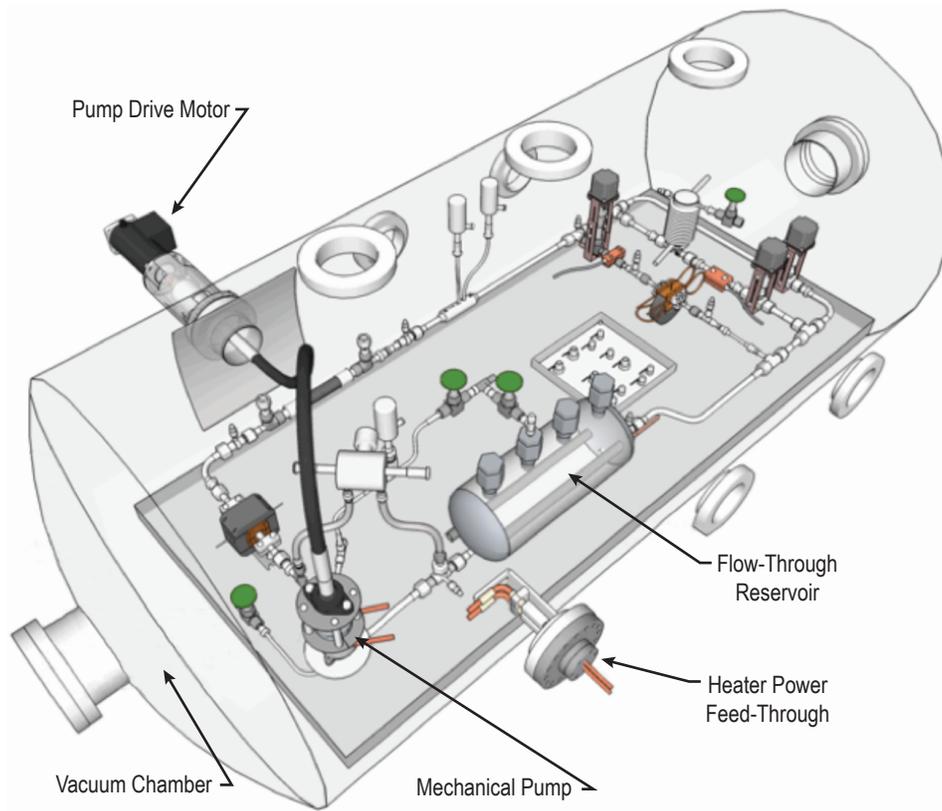
Figure 3.  FTL arrangement in vacuum chamber.

Argon (Ar) is used as the cover gas for the liquid metal in the circuit. When applied through the reservoir, it serves as head pressure for the mechanical NaK pump. A separate volume of Ar is used to prevent NaK from migrating into the top coupling of the mechanical pump. It is continuously monitored for temperature and pressure during testing, as shown in figure 4.

A three-line $GN_2$ system interfaces with the FTL to provide cooling in three locations: in the liquid metal-to-gas HX, the plugging valve, and the cold trap. The $GN_2$ lines all vent to atmosphere outside the high bay where testing takes place.

In addition to the primary system graphite-heating element, several small resistance-heating elements are individually controlled to provide heating at discrete positions throughout the loop. The graphite heater element provides bulk heating of the NaK and is controlled via DC power supply. The smaller elements are located to counter heat sinks throughout the system and provide isothermal performance at steady-state conditions. These smaller elements operate on 110 VAC.

A complete system schematic is provided in appendix A.
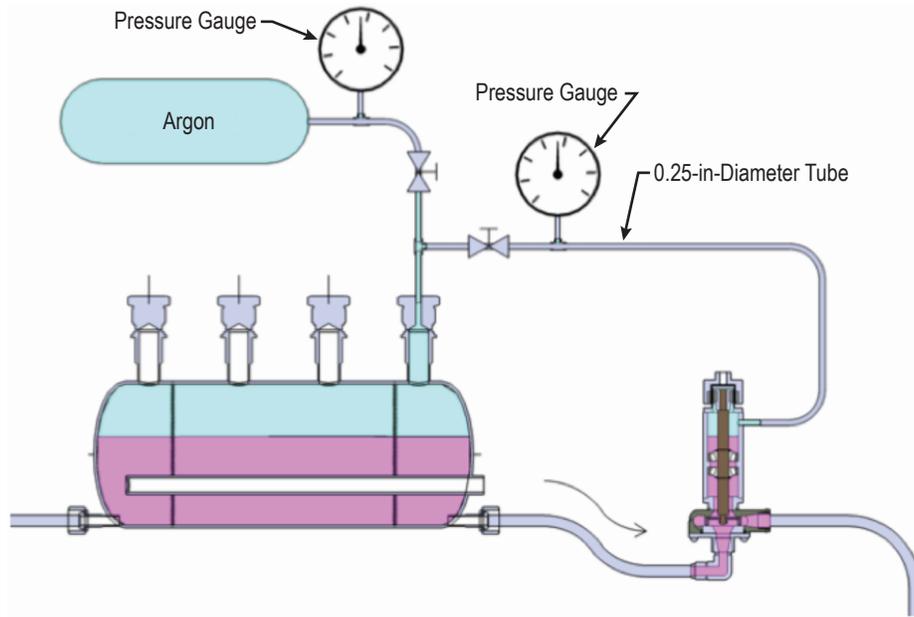
Figure 4.  Argon cover gas arrangement.

## 2.2  Feasibility Test Loop Components

### 2.2.1  Heated Flow-Through Reservoir

Electrical heat is input to the FTL through the loop reservoir, simulating the heat of fission. While this design is not prototypical of a flight system, it fulfills three important roles for testing in a relatively small vacuum chamber: (1) A reservoir for application of a blanket gas to preclude pump cavitation, (2) a reservoir to allow for expansion of heated NaK, and (3) reduction of the overall footprint by integration of heaters. The reservoir has an internal volume of ≈8 L and is equipped with two all-welded horizontal ports sized to receive approximately 0.63-in- (1.6-cm-) diameter by 16-in- (40.64-cm-) long graphite resistance heater elements capable of providing 3 kW each (see fig. 5). For this experiment, only one heater was used.

The loop operates with the reservoir half full of NaK. The horizontal ports are located such that they are fully submerged in NaK at all times during operation (see fig. 6). Heating is accomplished via radiation between the heating element and the SS port, which then heats the NaK via forced convection as the NaK circulates through the loop and into the reservoir where it is forced to flow around the graphite heater.

In the EFF-TF, graphite heaters are thermally coupled to their housings—in this case, the horizontal ports in the reservoir—by back-filling the housing spaces with helium (He). However, it was determined that the heater power levels required for this test series were sufficiently low to render the use of He unnecessary. Thermocouples (TCs) were placed to measure the graphite heater port wall temperatures in order to maintain safe operation.

7
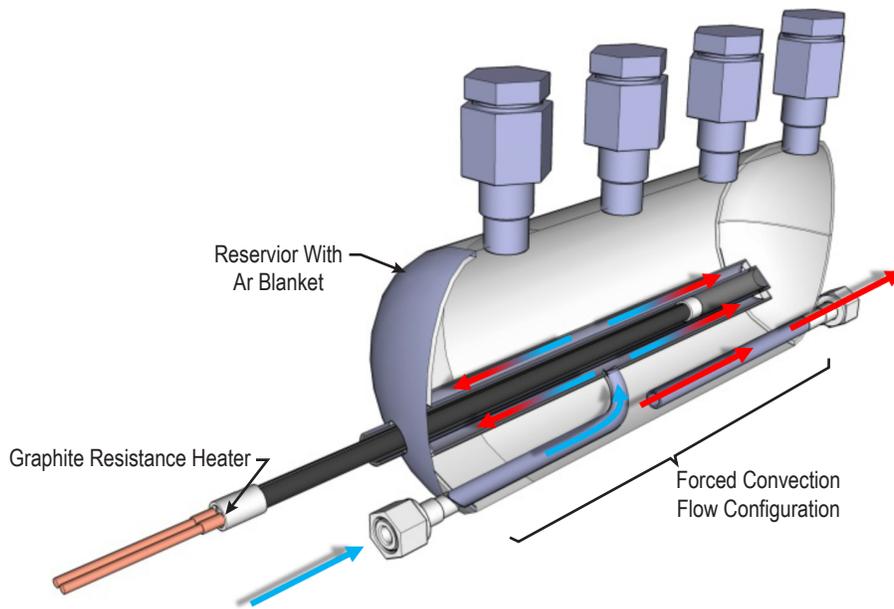
Figure 5.  Cutaway view of heated NaK reservoir.
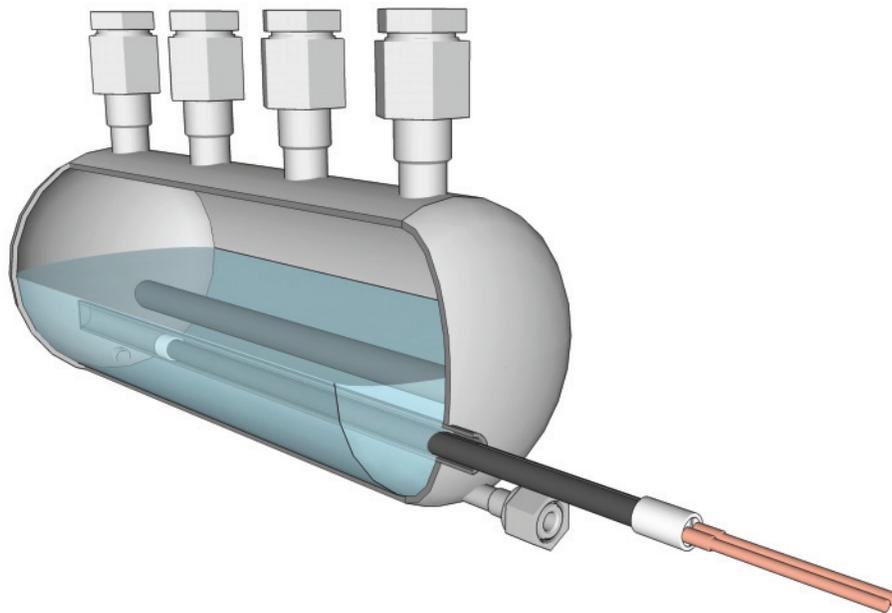


Figure 6.  Heated NaK reservoir cutaway view showing graphite resistance heater.

The reservoir is also equipped with four 1-in (2.54-cm) vertical access ports in addition to the two 0.5-in (1.27-cm) horizontal flow-through ports for NaK passage. Two level sensors are installed

in two of these vertical ports. The other two vertical ports provide for the Ar cover gas and a purge line to the cold trap to facilitate draining.

### 2.2.2 Mechanical Centrifugal Sodium-Potassium Pump

The NaK pump design must provide sufficient volumetric flow to facilitate component testing. Analysis of previous FTL testing data identified low volumetric flow to be a considerable obstacle to component testing. The previous FTL configuration employed an EM pump whose design flow rate was a maximum of 42 cc/s at nominal temperature with the actual hardware ultimately producing a maximum flow rate of 5 cc/s. With an estimated overall loop transit length of ≈3 m, this flow rate produced a loop transit time of roughly 1 min. This required a significant amount of time to achieve high operating temperatures, and resulted in difficulties in maintaining steady-state temperatures due to the high variability of NaK temperature around the loop. While the mechanical pump was not designed for a specific flow rate, it was expected to produce a minimum improvement of an order of magnitude, or a minimum of ≈55 cc/s.

The NaK pump employed in this testing was based on an off-the-shelf, all 316 SS water pump housing and impeller by MP Pumps, Fraser, Michigan, shown in figure 7. The pump design was not intended to be flight-like, but rather to provide adequate performance to successfully achieve testing goals.



Figure 7.  MP Pumps impeller and housing.

With the exception of these two components, the pump was fabricated in-house as a low-cost demonstration unit (fig. 8). With the manufacturer's pump performance curve and an analytical model of the loop using the Generalized Fluid System Simulation Program (GFSSP), the impeller/involute design was predicted to provide 3.5 gpm at 13 ft (3.96 m) of head. A full pump performance curve, as provided by the pump manufacturer, is included in appendix B.



Figure 8.  Mechanical pump assembly.

Two opposed, tapered roller bearing assemblies support the pump shaft. They are submerged in NaK for lubrication (fig. 9). The separation of the pump drive system and the pump body is accomplished using a magnetic coupling that transmits torque through the pump housing without any direct mechanical connection. A pump body cooling system consisting of clamped on water-cooling tubes, is provided to limit heat transfer to the drive magnets.

The magnetic coupling consists of neodymium rare earth magnets in two separate drive and driven connectors as shown in figure 10. The driven element is fully encased in SS. Argon is used as a blanket gas in the pump body to prevent NaK from contacting the magnetic coupling.

To employ a conventional DC motor outside the vacuum chamber, the drive connector is coupled to a DC motor via a support bearing, flexible drive shaft, and vacuum-rated rotary feed-through (fig. 11).

### 2.2.3  Flow Sensor Theory of Operation

A DC EM flow sensor was implemented into the plugging loop to monitor the change in flow rate as oxides precipitate out of the NaK solution and block the plugging meter holes. An idealized schematic of a DC EM flow sensor is presented in figure 12. The liquid metal flows though a channel of width ($w$), length ($l$), and height ($s$). The magnetic flux density ($B$) and time-varying flow rate ($u(t)$) are perpendicular both to each other and the direction across which the voltage ($v(t)$) is measured.

10
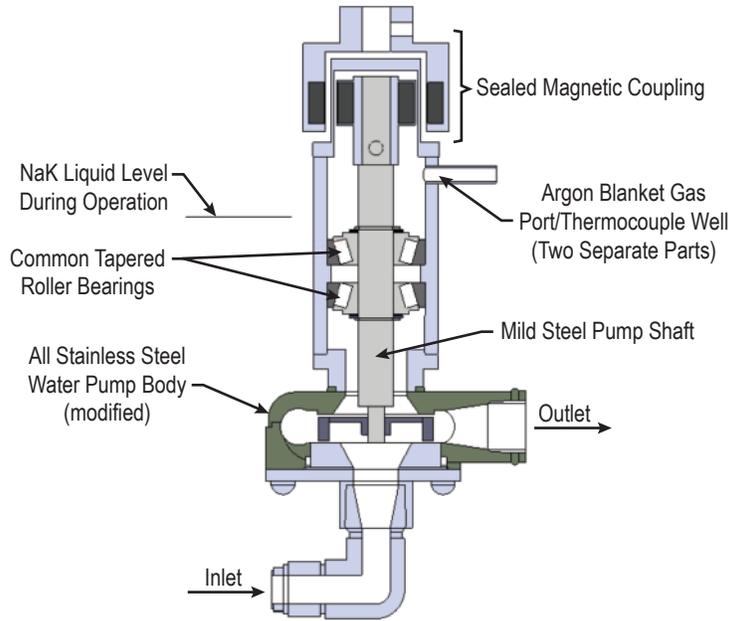
Figure 9. Mechanical pump cutaway.
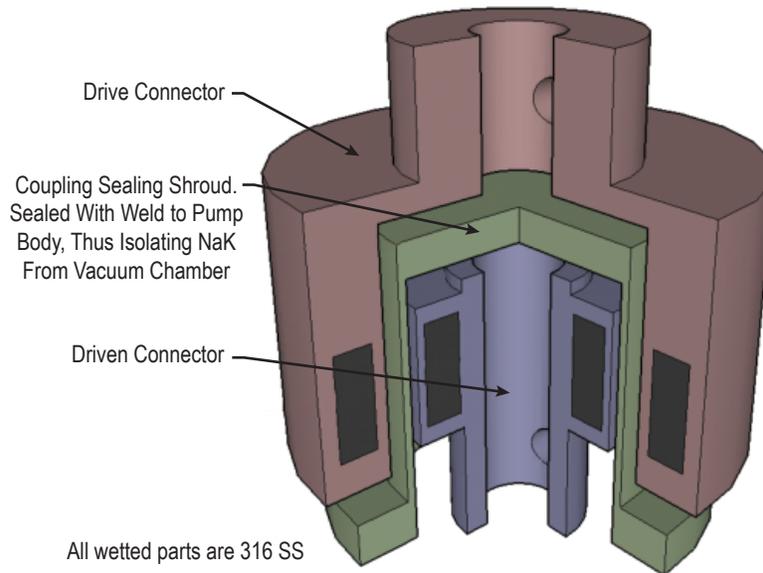


Figure 10. Mechanical pump magnetic coupling.

When an electrically conductive medium (a conducting liquid in this case) moves transverse to an applied field, a back-electromagnetic force (EMF) is induced according to the vector equation:

$$\vec{E} = -\vec{u} \times \vec{B} \ .$$

(1)
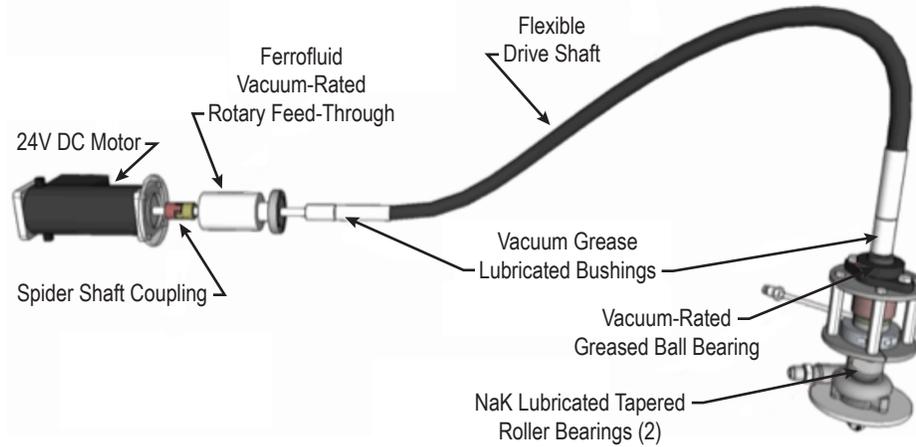
Figure 11. Mechanical pump drive system.
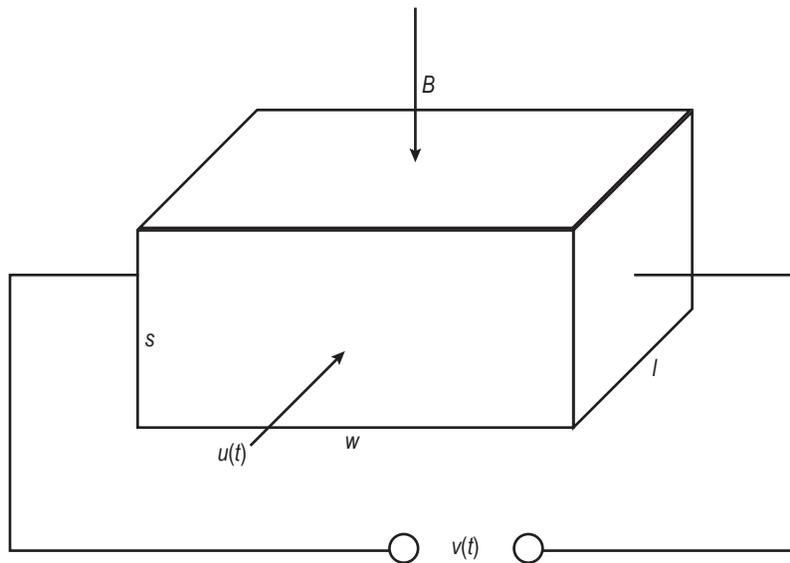


Figure 12. Electromagnetic flow sensor schematic.

Integrating the electric field over the width ($w$) (assuming spatially uniform values of $u$ and $B$ over the indicated faces), the voltage induced across the channel for a given mass flow rate, or the corresponding volumetric flow rate, is equal to

$$v = \frac{\dot{m}B}{\rho s} = \dot{V}\frac{B}{s} \ . \tag{2}$$

The voltage output by the flow sensor is linearly dependent on the ratio $B/s$, making even an absolute measurement relatively simple once the meter has been calibrated.

## 2.2.4 Electromagnetic Flowmeters

The FTL is equipped with two separate EM flowmeters. Electromagnetic flowmeters take advantage of fluid conductivity to generate an electrical EMF by vector cross product of fluid flow with an orthogonal magnetic field as shown in figure 13.
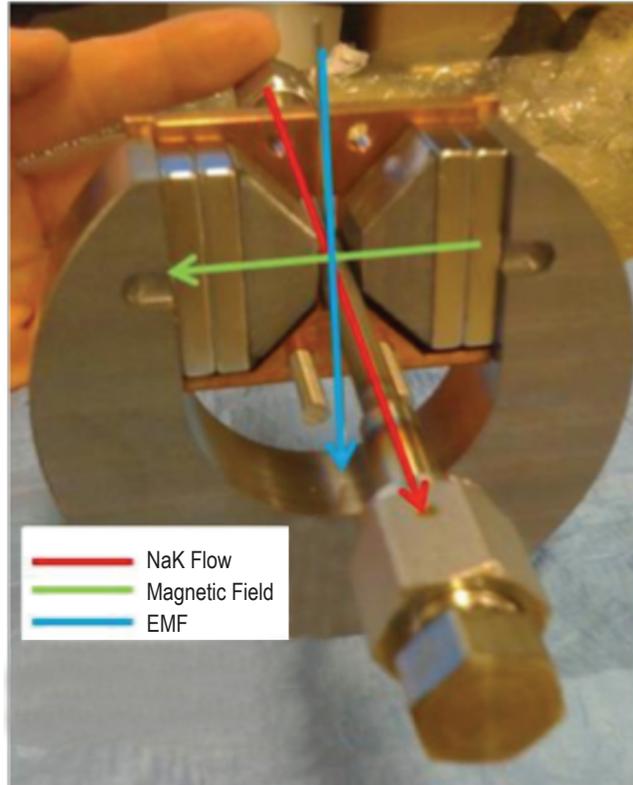


Figure 13.  Plugging EM flowmeter internals.

Because an EM flowmeter is a DC generator inducing an EMF, the electrical field strength is proportional to the following factors:

$$v = K\dot{V}\frac{B}{s} \;,$$

(3)

where

$v$ = signal voltage generated (mV)
$K$ = constant
$\dot{V}$ = volumetric flow of fluid (cc/s)
$B$ = magnetic flux density (T)
$s$  = ID of fluid-carrying conduit (cm).

The constant ($K$) provides for losses in the measured voltage associated with current shunting through the conductive walls of the NaK flow tube rather than through the NaK itself. An ideal flowmeter would have the entire current passing through the NaK or a factor of $K = 1$.

Flowmeter signals are generally very small (fractions of a millivolt), and are difficult to predict accurately from hardware geometry. Their chief advantage is output signal linearity with volumetric fluid flow rate. Electromagnetic flowmeters are generally calibrated using measured volumes of fluid captured in finite time periods (capture and count). The EM flowmeters use nickel-plated neodymium rare earth magnets with a magnetically permeable bale to complete the magnetic flow circuit. The configuration of the bale focuses the magnetic flux in the vicinity of the fluid flow tube in order to maximize signal output as shown in figure 13.

The flowmeters are equipped with water-cooled copper (Cu) blocks, which conduct heat away from the magnets. The cooling system protects the magnets but is primarily intended to maintain isothermal conditions so that consistent magnetic field strength is available at all temperatures.

Previous flowmeter configurations experienced signal variations due to expansion of loop tubing and consequent movement of the flowmeter NaK channel within the magnetic field structure. To ensure that the NaK channels remain stationary within their magnetic field structure, each flowmeter has a clamping mechanism provided to index all magnetic field structure relative to NaK flow tubing (fig. 14).
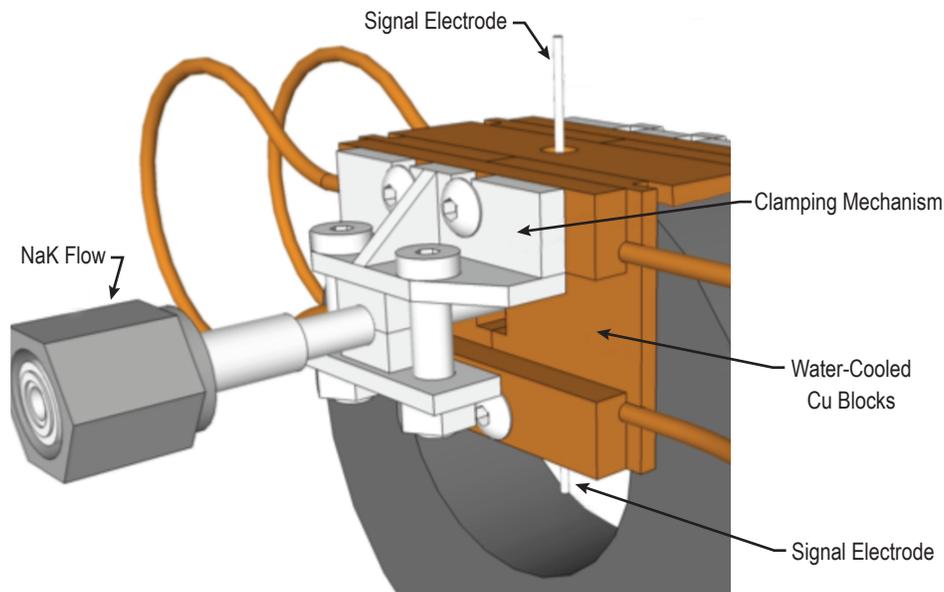


Figure 14.  Plugging flowmeter showing clamping mechanism.

**2.2.4.1  Main Loop Electromagnetic Flowmeter.** The main loop flowmeter records the total volume flow of NaK produced by the pump. The main loop flowmeter uses a design carried over from a previous FTL configuration with minor modifications.

The previous design used a NaK flow channel that transitioned from a full 0.5-in- (1.27-cm-) diameter tube to a flattened channel back to full diameter as shown in figure 15. The purpose of the flattened section was to allow the magnets in the magnetic field structure to have a minimal gap between them, and therefore the highest magnetic flux in the region of the NaK flow channel.
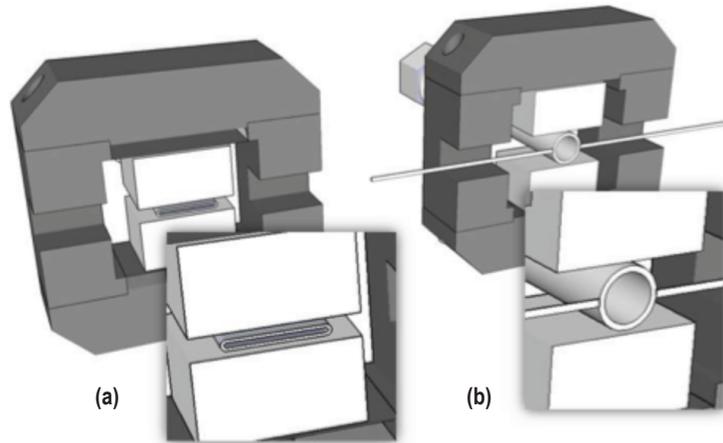


Figure15. Main EM flowmeter configuration changes: (a) old and (b) new.

The transition represents a cross-sectional flow area restriction of nearly 50%. The resulting hydraulic resistance trades poorly with the relative increase in magnetic field strength. As a result, the flowmeter design was modified to incorporate a full 0.5-in- (1.27-cm-) diameter tube throughout the magnetic field structure, resulting in a larger gap between the magnets. Simulations indicated that although the magnetic flux is reduced overall, the signal-to-noise ratio of the new design would be more than sufficient to record. The final, as-built main loop flowmeter can be seen in figure 16.

**2.2.4.2 Plugging Branch Electromagnetic Flowmeter.** The plugging branch flowmeter records only flow through the plugging branch of the loop. The plugging flowmeter is a complete redesign based on a desire to remove the magnets from the immediate vicinity of the heated NaK flow channel.

The smaller plugging branch flowmeter is designed to measure very low volumetric flow rates on the order of zero to 15 cc/s. A magnetic field modeling software analysis was performed to obtain magnetic field strength predictions as shown in figure 17. The field strength predicted by the model was 0.9 T in the vicinity of the NaK flow tube. Given that the flow tube is a nominal 0.25-in (0.64-cm) tube with 0.035-in (0.09-cm) wall thickness, and assuming an ideal flowmeter ($K=1$), then

$K = 1$
$B = 0.9$ T
$s = (0.25 \text{ in} - 2(0.035 \text{ in}) \times 2.54 \text{ cm/in} = 0.4572 \text{ cm}$
$\dot{V} = (1)(v)(0.9)/(0.4572) = 0.197*v(\text{cc/s}).$
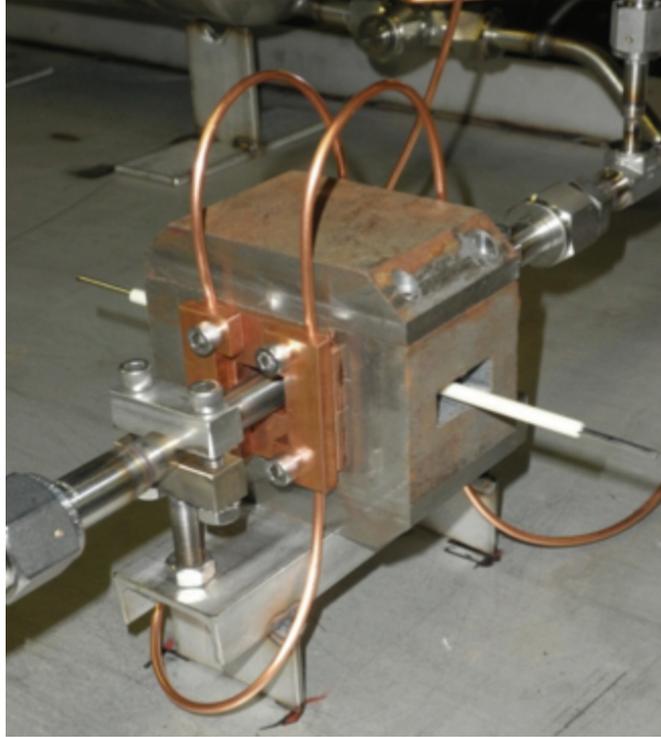
Figure 16.  As-built main loop flowmeter.

The resulting flowmeter predicted output is shown in figure 18.

### 2.2.5  Venturi Flowmeter

The venturi flowmeter was purchased from Preso Meters, Racine, Wisconsin. It consists of a flow section with a precisely defined profile equipped with two pressure taps, one upstream of the meter and one at the smallest restriction (fig. 19). By measuring the difference in the fluid pressures, the flow rate can be readily determined.

Given the wide variation of temperatures expected for operation, postprocessing of pressure readings is necessary to account for changes in fluid density and viscosity. The venturi flowmeter is implemented as a redundant and alternative flow measurement to EM flowmeters with the potential to act as a calibration reference. Pressure drop across a venturi meter has a quadratic relationship with volumetric flow rate (fig. 20).

Measurement of NaK flow is important as it ultimately represents an energy rate or power level when combined with fluid temperature. Electromagnetic flowmeters, which are relatively new technology, rely on principles of electrical induction to generate a measurable signal. The venturi flowmeter, on the other hand, relies on long-standing fluid flow principles in and around restrictions that have been proven and documented extensively. The venturi flowmeter therefore provides
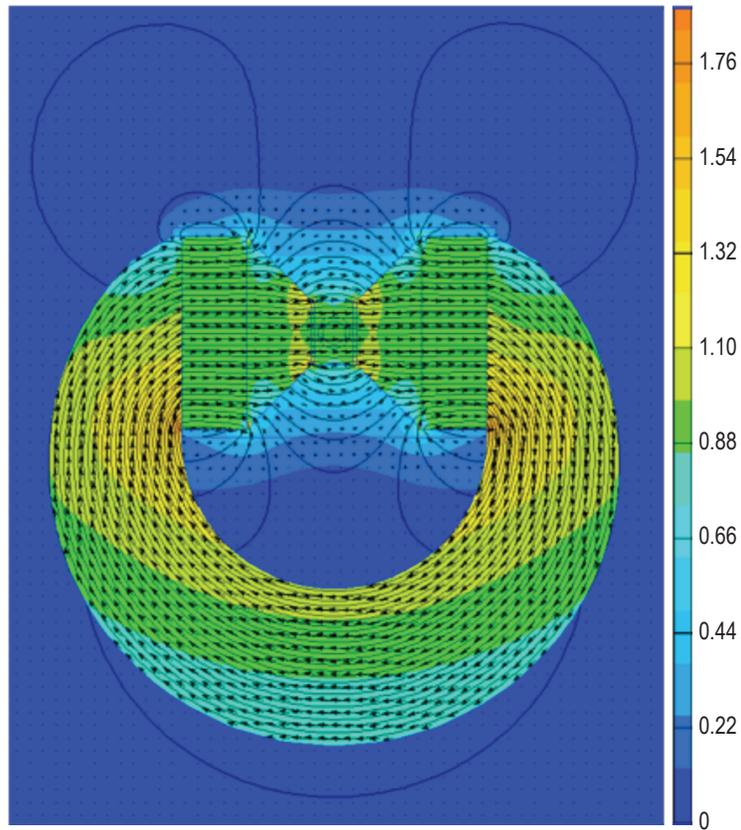
Figure 17.  Plugging flowmeter magnetic flux density model.
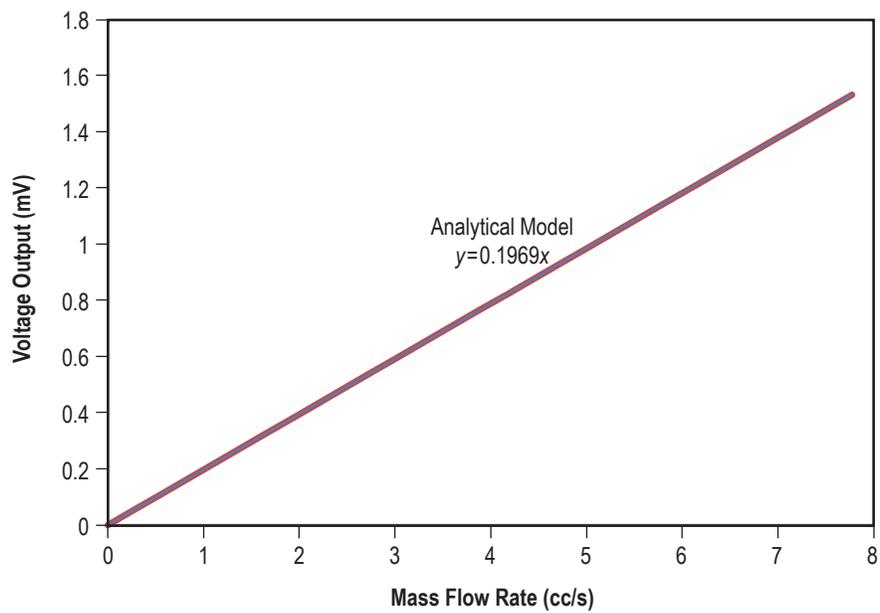


Figure 18.  Plugging flowmeter predicted signal output.
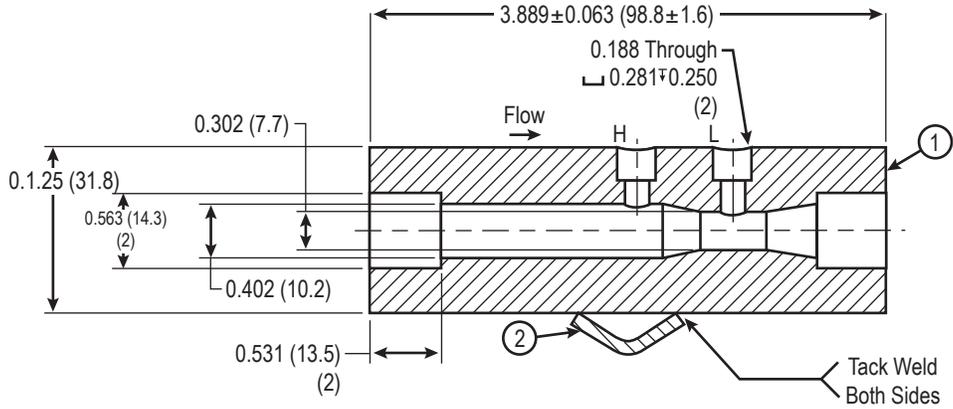
Figure19.  Preso venturi flowmeter section.
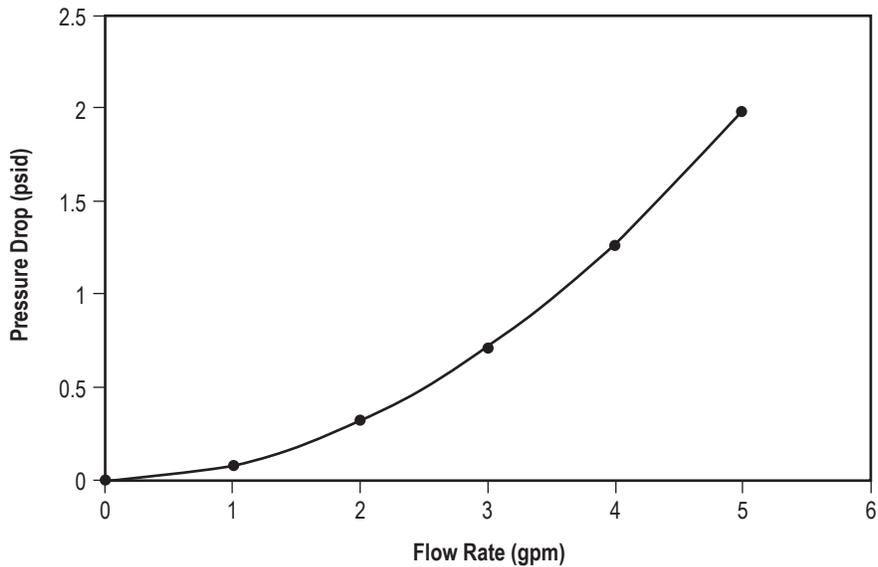


Figure 20.  Venturi flowmeter pressure versus flow rate.

a reference flow measurement that may be compared to the signal output of the EM flowmeter for performance confirmation and calibration when appropriate.

It should be noted, however, that venturi flowmeters are most accurate when designed to perform at very specific fluid flow conditions and suffer significant loss of accuracy when deviating from those conditions. The venturi flowmeter measurement relies on recording a pressure drop that is enabled by use of one or more pressure transducers (PTs). A low pressure drop is desirable so as to present minimal parasitic loss to system flow. A low pressure drop is difficult to record, however, so a performance tradeoff exists for a venturi flowmeter. If the venturi flowmeter in conjunction with its associated PT(s) is sized for best accuracy at the nominal system flow rate, it will generally suffer from signal inaccuracy at much reduced flow rates.

The EM flowmeter output signal, according to theory, should be zero at zero flow rate, rising linearly with increasing flow rate. The EM flowmeter signal may therefore be estimated by a straight line, $y = mx + b$ intersecting the $y$ axis at $(x,y) = (0,0)$. Any nonzero flow condition will provide a point on that line $(x1,y1)$ from which the slope, $m$, may be determined.

Assuming the venturi flowmeter is located in series with a given EM flowmeter so that all flow passing through it also passes through the EM flowmeter, the venturi flowmeter can be used to provide an operational data point for use in calibrating the EM flowmeter. The EM flowmeter thus calibrated can then be used at a full range of flow rates, which fall outside the accuracy regime of the venturi flowmeter.

### 2.2.6 Plugging Indicator for Contamination Measurement

When working with most higher temperature alkali metal systems, corrosion is a major concern. The primary contaminant of interest in a pumped NaK cooling system is O. Oxygen dissolves into NaK and forms sodium and potassium oxides. The saturation concentration of O dissolved in NaK versus NaK temperature is well known. See figure 21.[6]
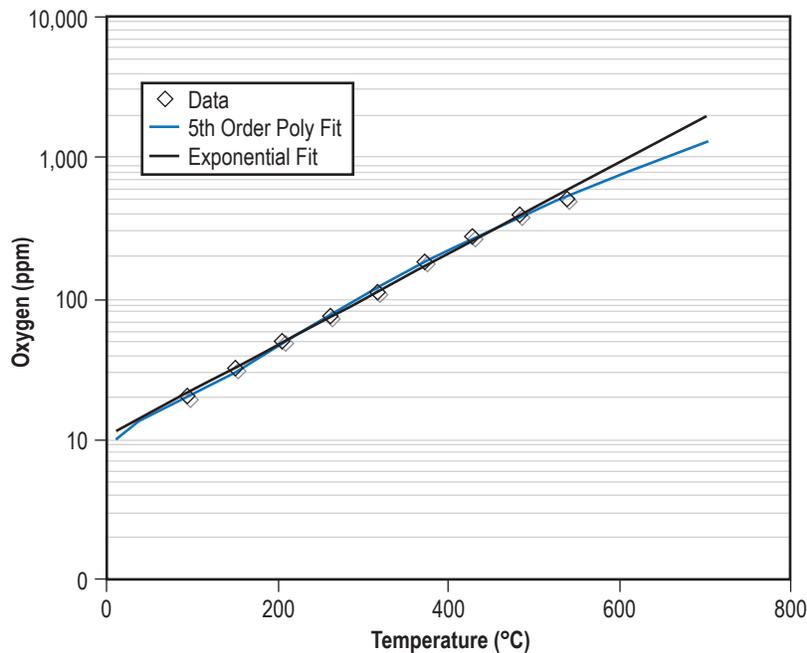


Figure 21.  Oxygen solubility in NaK.

Several methods of contamination measurement have been proposed.[6] For the purposes of the current FTL configuration, it was desired to characterize a plugging indicator as this was within both the technical and cost scope of the FTL.

The mechanism of plugging assumes O is present in the system. As the temperature of the NaK in the loop increases, O dissolves into the NaK solution. This process continues until all available O has been dissolved into solution, or the saturation concentration of oxides at the NaK temperature has been reached and no further dissolution of oxides is possible. As the NaK cools, the dissolved oxides precipitate out of solution.

A plugging indicator is the combination of an adjustable flow orifice, a mechanism for cooling the NaK solution, and a flow measuring device. The FTL plugging indicator consists of a flow-metering valve, a $GN_2$ cooling block, and the plugging EM flowmeter (fig. 22).
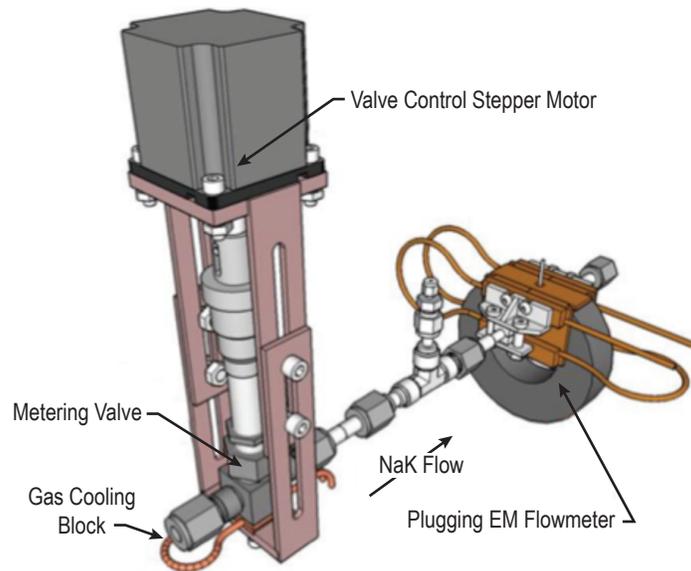


Figure 22. Plugging indicator.

At a steady rate of flow, the NaK solution is slowly cooled, causing oxides to precipitate in the adjustable orifice. During this cooling process, the flow rate is observed. The 'plugging' event is identified when flow rate through the device drops dramatically. See figure 23.

Comparing the solubility curve for O in NaK with the measured temperature of the NaK solution at the time of the plugging provides an oxide contamination concentration. By discontinuing cooling and adjusting the orifice to increase its cross-sectional flow area, the precipitated oxides may dissolve back into the heated NaK solution, permitting reuse of the plugging indicator.

### 2.2.7 Cold Trap for Online Sodium-Potassium Purification

The mechanism for purification is similar to that of the plugging indicator. As NaK is cooled, any dissolved oxides precipitate out of solution. This mechanism is used to force precipitation to occur in a containment filter known as a cold trap (fig. 24). The oxides then can be captured by placing a material with a large surface area in contact with the NaK solution and providing cooling in the same region.
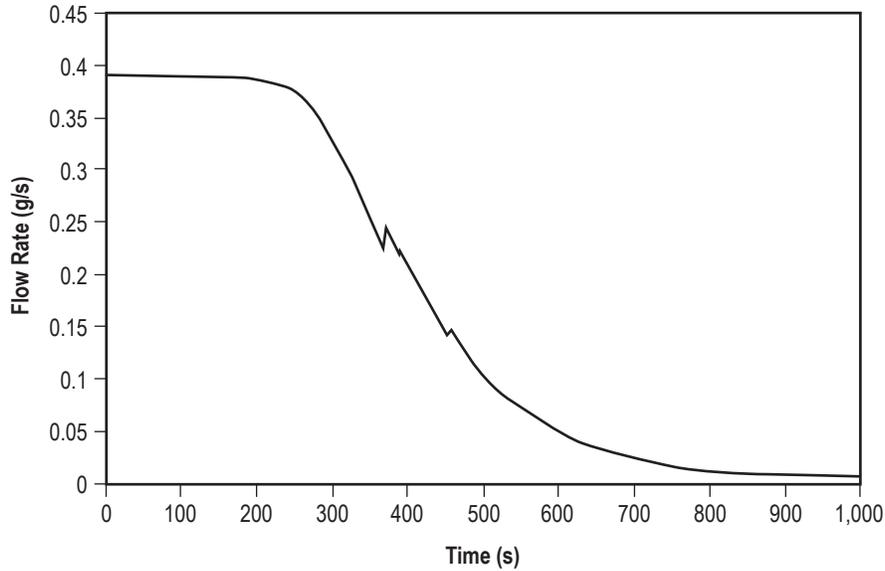
Figure 23.  Sample plugging flowmeter output during plugging.
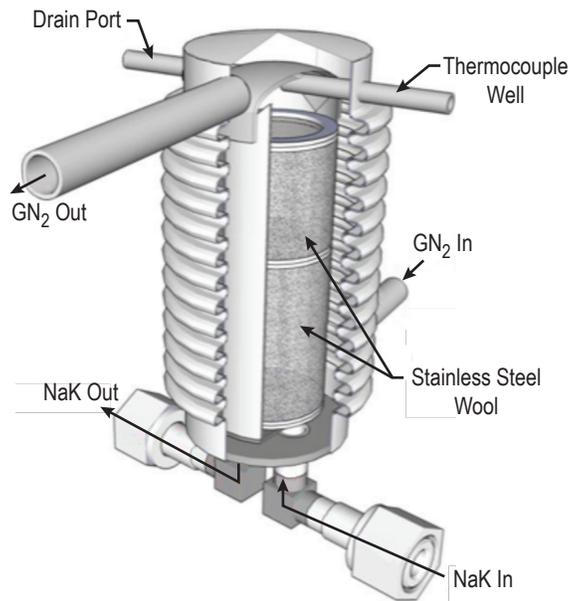


Figure 24.  Cold trap overview.

The cold trap is cooled by flowing $GN_2$ around the outer surface of an annular, counterflow NaK economizer. Within the economizer are two SS wool filters of different densities that provide maximum surface area for solid precipitation. See details in figures 24 and 25.

The available surface area in the cold trap defines the total oxide quantity that can be removed. The rate of O removal is dependent on cooling capacity and NaK latency within the trap. The longer

**(1)** Hot NaK enters trap.
**(2)** NaK flows down outer annulus and is cooled by $GN_2$ in jacket and cooled NaK flowing inside opposite.
**(3)** Coolest NaK.
**(4)** NaK passes through stainless steel wool depositing oxides.
**(5)** NaK exits trap.
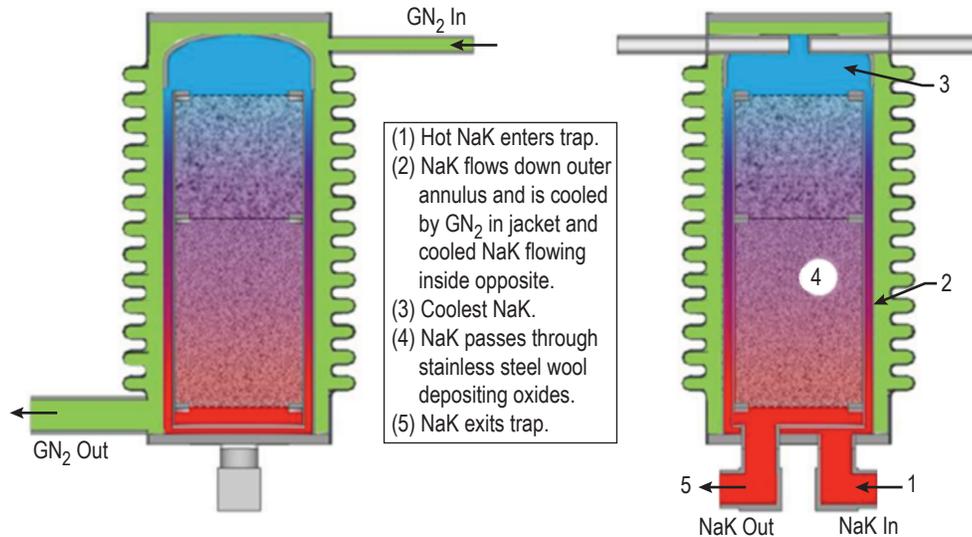
Figure 25. Cold trap economizer detail.

the NaK solution is in contact with the cool material, the greater the amount of O that is removed (in the form of precipitating oxides). A flow control valve is provided to regulate NaK latency within the trap.

Note that in order to restrict the precipitation of oxides to the cold trap (and nowhere else in the NaK flow path), it is important to tightly control the temperature of the solution such that it is the same at the inlet and exit of the trap, but drops to a significantly lower level within the cold trap. The economizer is included to reheat the NaK as much as possible as it exits the cold trap. Furthermore, a resistance heater is located downstream of the trap to minimize further oxide precipitation outside of the trap. See figure 26.

### 2.2.8  Pressure Transducers

There are five separate PTs in use in the FTL (table 1).

Pressure transducers PT-02 and PT-03 are associated with flow rate measurement by the venturi meter (fig. 27). Cooling water coils were applied to these transducers to combat thermal drift. Thermal drift has been identified as an issue during longer duration testing where PTs are exposed to radiation heat transfer from the NaK loop (fig. 28). This effort is similar to that of cooling the magnets in the EM flowmeters.

### 2.2.9  Temperature Measurements

Temperature measurements are made throughout the system with type-K, ungrounded TCs. A complete summary of TC locations is provided in appendix C. The TCs are clamped in place using several different methods as necessary to obtain useful measurements (figs. 29–32).
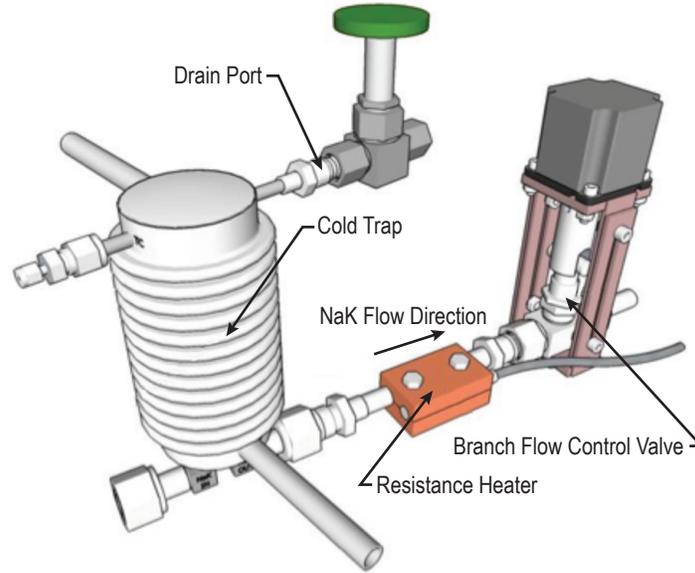
Figure 26.  Cold trap branch details.

Table 1.  FTL pressure transducers.

| ID | Type | Location | Fluid | Range | Vendor |
|----|------|----------|-------|-------|--------|
| PT-01 | Absolute | Reservoir Ar gas blanket pressure | Ar | 0–100 psia | MKS |
| PT-02 | Absolute | Venturi upstream pressure | NaK | 0–25 psia | Delta Metrics |
| PT-03 | Absolute | Venturi throat pressure | NaK | 0–25 psia | Delta Metrics |
| PT-04 | Absolute | Mechanical NaK pump Ar gas pressure | Ar/NaK | 0–50 psia | Delta Metrics |
| DP-01 | Differential | Mechanical NaK pump inlet/outlet | NaK | +7 psid | Delta Metrics |
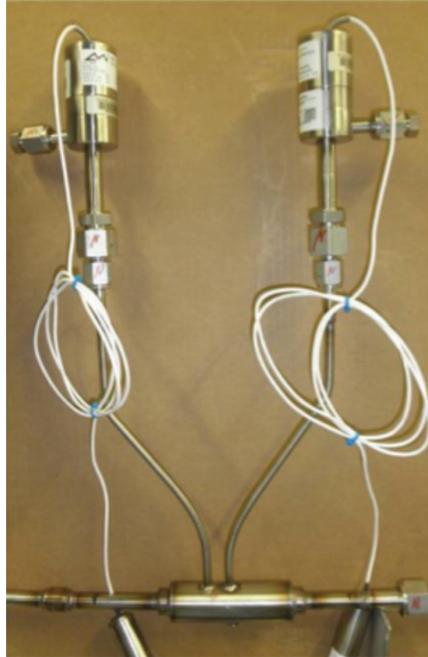
Figure 27.  Venturi flowmeter with absolute PTs.
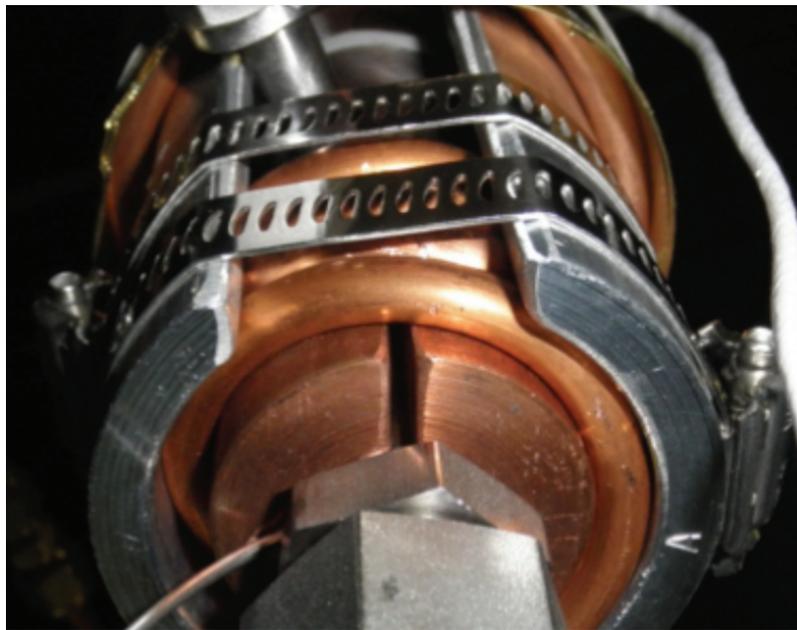


Figure 28.  Pressure transducer cooling water coils.

Figure 29.  Thermocouple clamped via cable tie with Cu foil (for 1/8-in (0.32-cm)
Cu water cooling tubes).
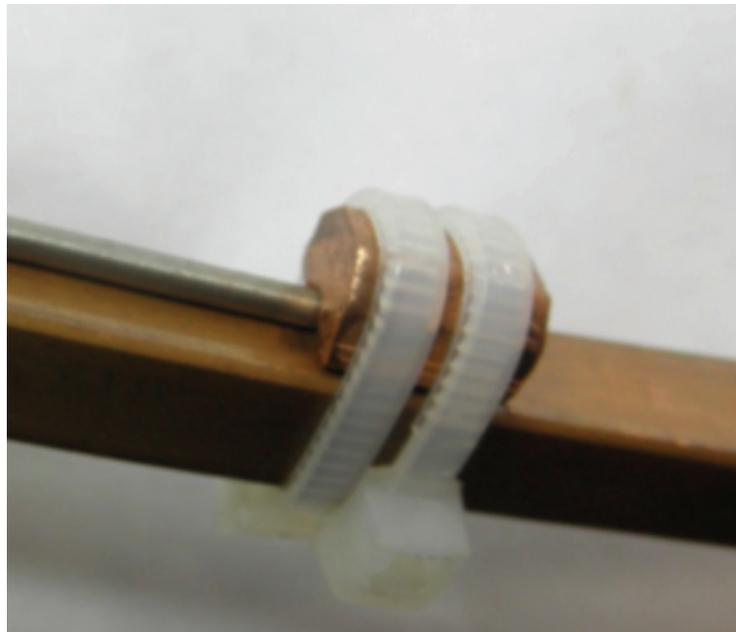


Figure 30.  Thermocouple clamped via cable tie with Cu block (for square Cu
water cooling lines).

### 2.2.10  Motor-Controlled Valves

NaK flow in the loop is regulated by a combination of three motor-controlled valves. The control motors are vacuum-rated stepper motors. The three valves allow flow diversion through any combination of three paths: the main loop, the plugging loop, or the cold trap (fig. 33). NaK nominally flows through the main loop bypass branch controlled by the motor valve (MV). NaK may be allowed to flow through the cold trap motor valve (CTMV) or the plugging motor valve (PMV).

In a simulated operational environment, the NaK flows nominally through the MV and is warmed via the heated flow-through reservoir. At a given steady operational temperature, the plugging branch may be opened to perform an oxide measurement or the cold trap branch may be opened to remove oxides from the NaK.
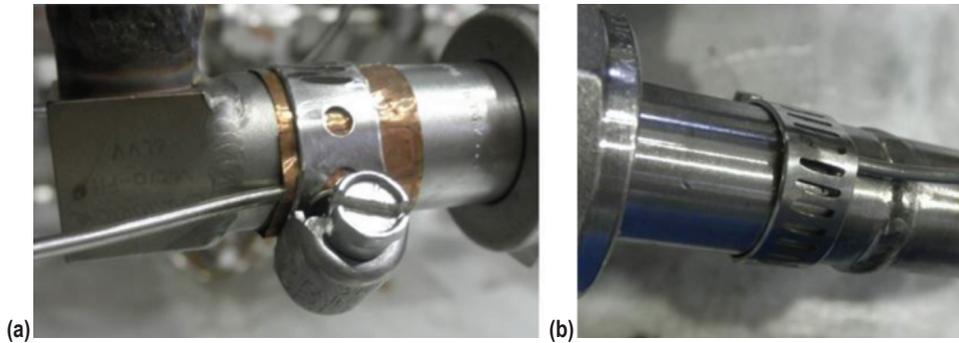
Figure 31. Thermocouple clamped via hose clamp (a) with and (b) without Cu foil (on SS tubing and/or fittings).



Note: Thermocouple proximity to flowing NaK
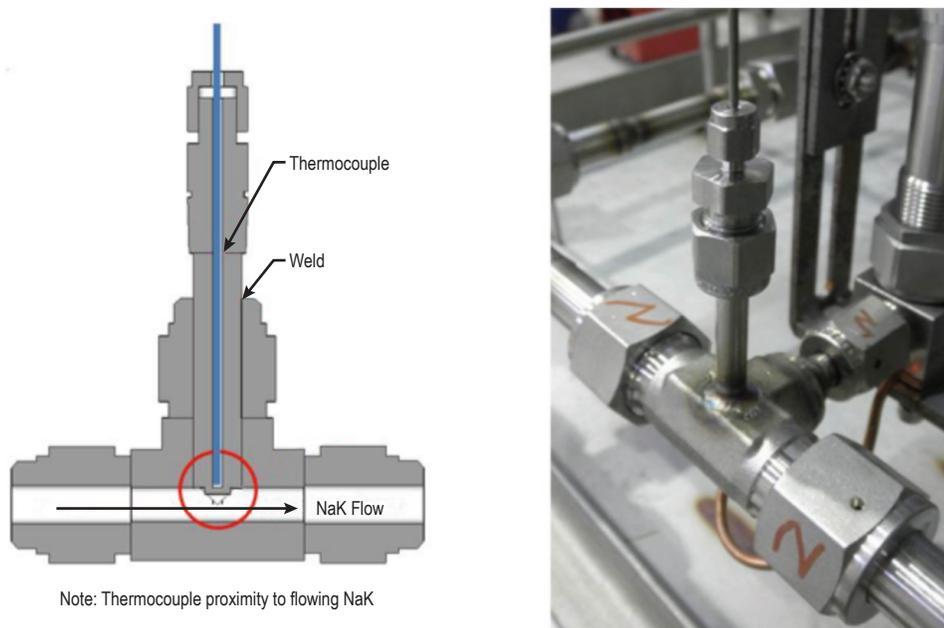
Figure 32. Thermocouples clamped as part of thermal well using Swagelok® fittings, which are strategically located at major heat inputs and sinks throughout the primary NaK loop.

## 2.2.11  Data Acquisition and Control Platform

The data acquisition (DAQ) and control system is based on National Instruments hardware and software. The system consists of a Windows XP-based PC for user interaction and data recording, a PXI-1042 chassis for DAQ and control, and an SCXI-1001 chassis for signal conditioning.

The PC runs an in-house-developed LabVIEW™ application that communicates via Transmission Control Protocol/Internet Protocol with the real-time LabVIEW application running on
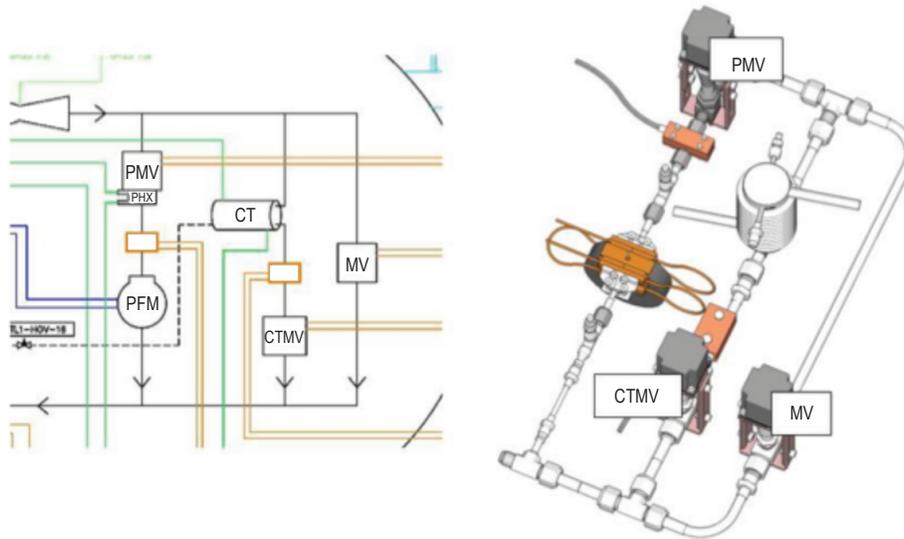
Figure 33.  Control valve locations.

the controller in the PXI-1042 chassis. The PC application receives data and status information for presentation and recording and transmits user-initiated commands to the controller in order to operate the experiment. The application provides a user interface for operating the heaters, valves, HXs and data recorder. It also presents the data acquired from the system and provides visual feedback on the status of the system. The PXI-1042 chassis includes a PXI-8110 Real-Time (RT) embedded controller, a PXI-6281 DAQ module, a PXI-6704 analog output module, a PXI-6528 digital input/output (I/O) module, and a PXI-6521 industrial digital I/O module. The PXI-8110 has a 2.26-GHz quad-core processor running the LabVIEW RT operating system. The controller runs an in-house-developed LabVIEW RT application that acquires data through the PXI-6281 DAQ module, scales the data into engineering units, monitors the data for alarm conditions, and transmits the data to the PC application for recording and display. The RT application also controls the operation of theexperiment in direct response to commands from the PC application and provides appropriate feedback status to the PC application. Any closed-loop control is handled by the RT application. The PXI-6281 DAQ module is used to scan all available channels from the SCXI-1001 chassis, which handles all signal conditioning.

The SCXI-1001 chassis includes SCXI-1102 analog input modules, an SCXI-1503 resistance temperature detector (RTD) analog input module, and an SCXI-1520 universal strain gauge input module. The SCXI-1102 module is used to condition analog voltage signals from various instrumentation transducers, including TCs and PTs. The SCXI-1503 RTD module is used to condition readings from an RTD, which measures the temperature of a TC cold junction located on the test rig inside the vacuum chamber. The SCXI-1520 is used to condition the signals from full-bridge strain gauge-based PTs. The NaK PTs originally featured signal conditioning amplifiers, which were located near the transducers inside the chamber. During testing it was determined that the amplifiers were overheating. The amplifiers inside the chamber were removed and replaced with the SCXI-1520 module outside the chamber.

# 3. TEST PROCEDURE AND RESULTS

While the ultimate goal of testing was to show flow loop contamination and purification via a plugging meter and cold trap, continuous, long-term efforts were required to research, design, assemble, and test several subscale components in order to successfully complete testing. The FTL test procedure began with preliminary individual subsystem tests of each of the major components. These were proof-of-concept tests for both new designs and component design iterations. Upon successful testing of individual components, increasing levels of control, integration, and operational temperature were imposed to verify or revise operational procedures. Once these procedures were verified, contamination and purification testing began. This required a minimum of two contaminant measurements from a higher to a lower level of contamination performed before and after a minimum of one online purification operation.

## 3.1 Test Matrices

The following tables list test descriptions of the various subsystems at three different temperature ranges (tables 2–4).

Table 2. Low-temperature (25 ºC) test matrix.

| Component or Subsystem | Test Description |
|---|---|
| Mechanical pump | Demonstrate flow of NaK through main loop. Demonstrate speed control and repeatability. |
| Venturi flowmeter | Demonstrate $\Delta P$ correlation with varied flow rate. |
| Motor-controlled valves | Demonstrate ability to remotely control NaK flow through all flow branches while under chamber vacuum. Demonstrate repeatability of valve setting. |

Table 3. Mid-temperature (25 to 150 ºC) test matrix.

| Component or Subsystem | Test Description |
|---|---|
| In-reservoir heater | Demonstrate ability to regulate power input. Demonstrate ability to heat entire loop via pumped circulation. |
| EM flowmeters | Demonstrate 'wetting' of flowmeters using 100 °C (212 °F) NaK flow (observe and record signal change). |
| Flow measurement calibration | Calibrate EM flowmeters using venturi flowmeter. Confirm flow rates via advance of temperature front in primary NaK loop. |

It is the nature of research hardware that both physical and operational characteristics of the hardware are established during operation and are not strictly dependent on intended design. Testing therefore proceeds from low technical risk and advances to increasing complexity based on operating criteria established during testing.

Table 4.  High-temperature (25 to 550 ºC) test matrix.

| Component or Subsystem | Test Description |
| --- | --- |
| Plugging indicator | Demonstrate flow-through plugging branch.<br>Record plugging event with main loop at steady-state temperature.<br>Clear plugging indicator for reuse. |
| Cold trap | Operate primary loop at temperature.<br>Operate cold trap branch to remove oxides. |
| Mechanical pump | Pump performance and endurance at increasing temperatures of operation. |

Low-temperature testing was conducted for major mechanical components as proof of concept and to establish operating procedures.

Mid-temperature testing established control procedures for the loop heating system and identified low-temperature performance dependence on temperature for flowmeters.

High-temperature testing represented prototypical, full-scale system operational characteristics simulating a NaK-cooled fission reactor. Testing provided proof of concept for oxide measurement and coolant purification via plugging and cold-trapping.

### 3.2  Testing Results

### 3.2.1  Mechanical Pump

The mechanical pump successfully provided NaK flow rates as high as 1.8 gpm or ≈115 cc/s. By comparison, previous FTL testing using an EM NaK pump achieved maximum flow rates of ≈5 cc/s.

A sample of performance data is provided below. Flow of NaK through the primary flow loop by record of a change in pressure rise across the pump as measured by DP-01 is shown in figure 34. Two separate runs from full stop to full speed indicated the same pressure rise, confirming speed control repeatability.

Using the resulting pressures from the venturi flowmeter, the calculated flow rate produced by the pump was 1.51 gpm at 4.4 psid (11.7-ft (3.57-m) head). This is in contrast to the pump performance curve that predicts 3.5 gpm at 13 ft (3.96 m). This difference reflects substantial deviation of the as-built flow system from the predicted GFSSP model. The actual system provided substantially more flow resistance than originally modeled. In addition, modifications to the pump for service in NaK (instead of water) may have altered the impeller/involute efficiency (fig. 35). Physical performance loss is most likely due to undesired flow between the high- and low-pressure sides of the impeller. During the pump modification process, the impeller and involute clearances were both altered and a mechanical seal was removed. This introduced an alternative flow path for accelerated fluids within the pump.

The mechanical pump design successfully achieved performance objectives and provided robust operation for subsequent successes in testing other system components.
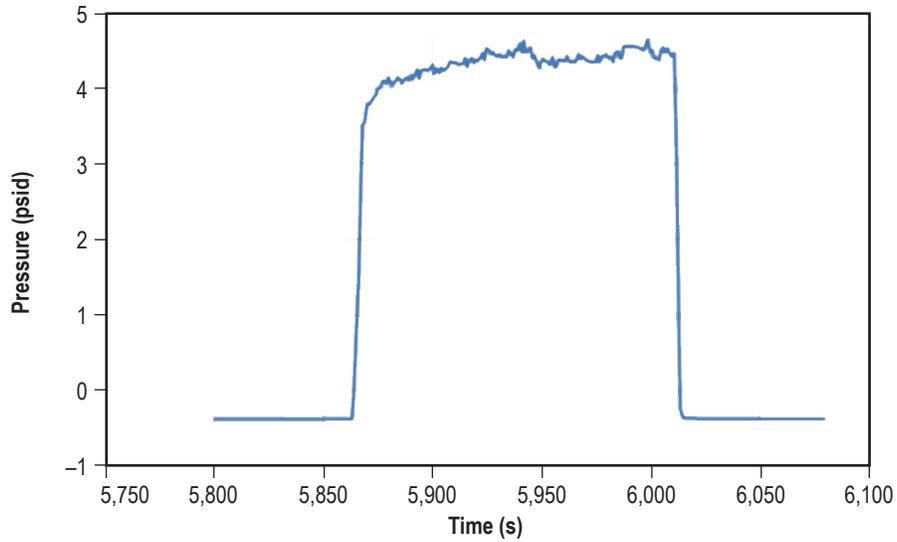
Figure 34.  Mechanical pump $\Delta P$ versus time.
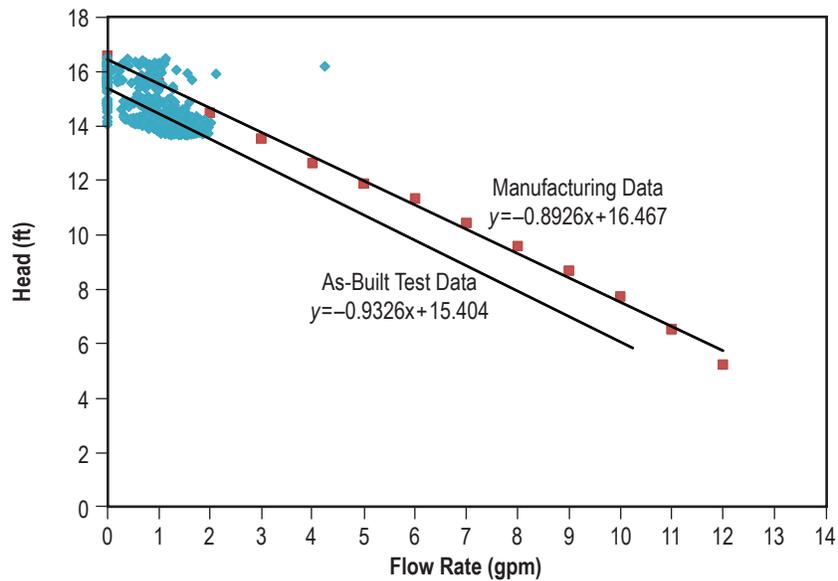


Figure 35.  Mechanical NaK pump performance curves.

As a result of this successful testing and due to lower-than-expected efficiencies in larger scale system EM NaK pumps, there was considerable interest in the overall efficiency of the mechanical NaK pump.

While the mechanical pump successfully increased the flow rate of the old EM pump, it is interesting to note that overall pump efficiency was very poor. Data analysis was performed to determine overall pump efficiency as built. A typical nominal operating point of 1.3 gpm at 14.1 ft (4.3 m)

was selected for the calculation. It should be noted that some of the power losses calculated in table 5 were not easily verified by test and should be used as estimates only.

Table 5. Power loss calculations.

| | |
|---|---|
| Power measured at DC motor input | 134.8 W |
| Efficiency of DC motor (from manufacturing data) | 81% |
| Motor power delivered to pump drive train | 134.8W×0.81=109.2 W |
| Power loss due to friction torque in single-row, greased ball bearing (estimated calculation) | –7.7 W |
| Power loss due to friction torque in bronze bushings (estimated calculation) | –22.4 W |
| Power loss due to flex shaft (obtained by test) | –16.7 W |
| Power loss due to friction torque at vacuum rotary feedthrough (from mfg, verified by test) | –18.5 W |
| Total power delivered by drive train to pump impeller shaft | 43.7 W |
| Total fluid power as measured from NaK flow and pressure rise data | 3 W |
| Net efficiency of pump as tested | 3 W/43.7 W=6.9% |

According to the MP Pumps performance specifications, the pump would be expected to have an efficiency of ≈9.6% at the operational point considered above. Manufacturer's efficiency data are based on their testing of an unmodified pump as would typically be delivered. The pump used in this FTL testing required some modification for use in NaK. The resulting difference in as-delivered versus as-tested efficiency is therefore due to these modifications or the estimates used in the calculations as noted above. The demonstration unit utilized in this testing used the same pump impeller and involute design as delivered and was selected purely on the basis of material and inlet/outlet port size compatibility. As a result, the pump was poorly matched to the test loop and therefore operated at low efficiency.

For reference, the pump was equipped with a six-vane, 1.6-in- (4.06-cm-) diameter impeller. It was ultimately intended to operate at a design point of (8 gpm at 9.6 ft (2.93 m) at 3,600 rpm). At the operating point described above (1.3 gpm at 14.1 ft (4.3 m) at 3,600 rpm) the ideal, most efficient impeller design would be a three-vane design with a diameter of approximately 2 in (5.08 cm).[9] Given a close-coupled motor without extensive drive train components and basic engineering rigor in the design of the pump impeller, efficiencies between 40% and 50% may be expected.

### 3.2.2 Venturi Flowmeter

Pressures recorded from the venturi flowmeter correlated well with the pump pressure rise. See figure 36. Calculations made using the net pressure difference between the upstream and throat pressure (estimated at 0.18 psid) indicate a flow rate of 1.51 gpm (fig. 37).

The venturi flowmeter was sized for an estimated maximum flow of 5 gpm as predicted from early system models. The as-built system, which deviated from that model substantially due to modifications resulting from early testing, represented a significantly higher flow resistance. The resulting reduction in overall flow rate did not negatively affect the overall testing goals but did limit the
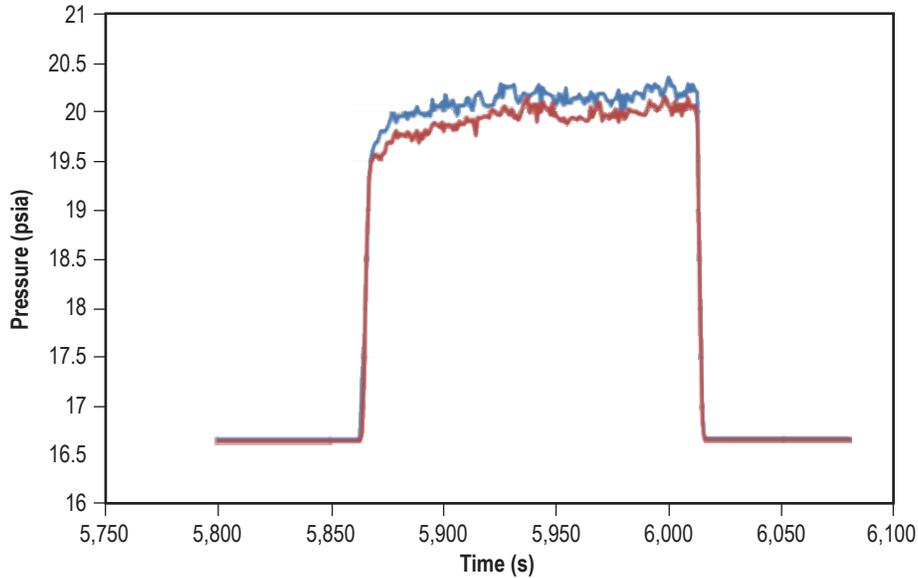
Figure 36.  NaK pressures at venturi flowmeter.

usefulness of the venturi flowmeter since its signal is decidedly nonlinear at lower flow rates and is also subject to greater PT line noise from mechanical vibration. The data provided by the venturi flowmeter provided a welcome confirmation of flow to provide redundancy to EM flowmeters and should be considered for all flow loops when properly sized for expected flow rates.

### 3.2.3  Electromagnetic Flowmeters

Both EM flowmeters provided ample signal-to-noise ratios and were subject to minimal temperature deviations due to their water-cooled magnets. Voltage signals could be calibrated to correlate with engineering units of gallons per minute and grams per second as required by testing. The use of full flow tubes did not observably affect the ability to measure flow and was therefore an excellent trade versus the loss of signal strength due to increased magnet separation. Water-cooling, while excellent for maintaining isothermal magnets and therefore constant magnetic field strength, had an undesirable effect as-built. The heat absorption provided by the water caused a net drop of NaK temperature as it passed through the flowmeter. The impact was particularly observed in the plugging flowmeter. During plugging tests, additional heaters were therefore provided along the plugging branch to compensate for this heat sink. In future testing, this issue could be eliminated by thermally isolating the water cooling from the NaK tubing or physically removing the magnets from the near vicinity of the heated flow tubes.

Sample data for the plugging flowmeter showing signal strength versus volumetric flow rate are provided below and include a comparison to predicted performance (fig. 38).

It should be noted that the plugging flowmeter output signal recorded during test was ≈60% of that predicted. The analytical model assumes an ideal flowmeter where all signal current passes only through the NaK in the flow tube. Given the similar conductivities of the 316 SS flow tube and

**FLOW RATE VS. DIFFERENTIAL PRESSURE**

(REFERENCING PRESO FLOW HANDBOOK)

5/31/11

| Value | Description |
|---|---|
| 25 | T, fluid temperature, °C |
| 866.7 | $\rho$, fluid density, kg/m³ (see sheet "NaK Density") |
| 0.8667 | $SG_f$, specific gravity of fluid (NaK) (water at 25°C = 1.0) |
| 0.628 | $\mu_{cp}$, fluid viscosity, Cp (see sheet "NaK Viscosity") (water at 25°C = 0.89 cP) |
| **0.1800** | $\Delta P$, differential pressure, psid |
| 4.9878 | Hw, differential pressure, inches of $H_2O$ at 68°F |
| 5.666 | N, units conversion factor (5.666 for GPM) |
| 0.75 | $\beta$, Venturi throat to tube inner diameter ratio |
| | K, Flow Coefficient |
| | SSL-1: 0.1215 |
| 0.6701 | SSL-2: 0.2436 |
| | SSL-3: 0.4259 |
| | SSL-4: 0.6701 |
| 0.402 | Di, tube inner diameter, inches |
| 0.3015 | Dv, venturi throat diameter, inches |
| 0.9996 | Fa, thermal expansion correction factor (see sheet "Fa") |
| 16348 | Re, Reynolds Number |
| | Fre, Reynolds Number Factor (for flow in pipe) |
| | Fre=1.0000 for 100,000 < Re < 1,000,000 |
| 1.0250 | Fre=1.0250 for Re < 100,000 |
| | Fre=0.9985 for Re > 1,000,000 |
| 1.0742 | Fsgf, Flowing Specific Gravity Factor |
| 0.6753 | C1, coefficient |
| 0.9850 | $C_D$, discharge coefficient |
| **1.508** | Q, flow rate, GPM |
| 0.182 | mdot, mass flow rate, lbm/sec |

$$Q = C1\sqrt{Hw}$$

$$Hw = (Q/C1)^2$$

$$C1 = N \cdot K \cdot Di^2 \cdot Fa \cdot Fre \cdot Fsgf$$

$$Re = \frac{3160 \cdot Q \cdot SG_f}{Di \cdot \mu_{cp}}$$

$$Fsgf = \sqrt{\frac{1}{SG_f}}$$

$$\dot{m} = Q\left(\frac{1\,\text{min}}{60\,\text{sec}}\right)\left(\frac{0.1336806\,\text{ft}^3}{1\,\text{Gal}}\right)\rho_{H_2O} SG_f$$

| SSM / SSL VENTURIS (ALL SIZES) | | |
|---|---|---|
| MODEL | BETA RATIO | K FACTOR |
| | | |
| SSM/SSL-1 | .35 | .1215 |
| SSM/SSL-2 | .49 | .2436 |
| SSM/SSL-3 | .63 | .4259 |
| SSM/SSL-4 | .75 | .6701 |
| | | |

$$\kappa = \frac{C_D \beta^2}{\sqrt{1-\beta^4}} \qquad C_D\,(\text{Discharge Coefficient}) = .985$$

Figure 37. Venturi flowmeter flow rate from $\Delta P$ sample calculation from Preso Flow Handbook.

the NaK, current shunts partially through the SS wall. The 40% loss of predicted signal strength may be reasonably attributed to this effect.

### 3.2.4 Contamination Measurement and Purification

Online O contamination measurement and purification were successfully demonstrated. For the purposes of testing, a plugging routine was defined as a complete evolution performed at steady main loop temperatures whereby the plugging indicator was slowly cooled and dropoff of flow rate observed from a baseline flow rate to zero flow. Several separate plugging routines were performed without any external modifications that could affect O content in the loop.

A cold-trapping routine was defined as a deliberate cooling of main loop NaK in the specially designed cold trap branch. Main loop temperature was maintained at a steady-state temperature above the identified prepurification plugging temperature to ensure oxides in the main loop were fully dissolved. The cold trap was maintained at a steady temperature delta from the main loop of
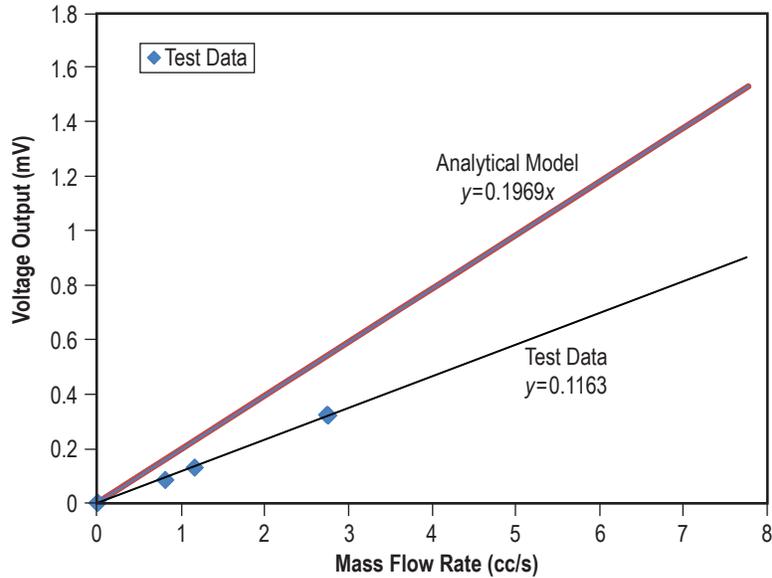
Figure 38.  Plugging flowmeter signal output data.

approximately 40–50 °C (104–122 °F). Flow was controlled such that ≈10% of the main loop flow passed through the cold trap. The above conditions were maintained for a full 30 min. For absolute purification at this temperature, an infinite amount of time would theoretically be required. The temperature delta and time duration were selected to reasonably demonstrate purification.

A definitive coolant purification cycle consists of the following:

- Prepurification O measurement via plugging routine.
- Purification via cold trap routine.
- Postpurification O measurement via plugging routine.

### 3.2.5  Plugging Operations

Several distinct plugging operations were performed. The test hardware allowed for real-time adjustment of operational parameters including:

- Cross-sectional flow area at plugging valve (and therefore initial NaK flow rate).
- Rate of cooling of plugging valve orifice via gas cooling combined with electric heating.

It was decided that the best opportunity to observe a plugging event and identify a precise plugging temperature would require a very shallow, steady temperature drop at the plugging valve, allowing for the slow and steady deposit of precipitates in the orifice.

The standard procedure employed for performing a plugging operation is as follows:

(1)  Open main loop bypass valve completely. Open plugging valve completely.

(2)  Preheat the plugging valve and as much of the plugging branch as possible. (At all times when flowing leading up to a plugging event, the plugging branch should be maintained at or above the main loop temperature so that plugging does not occur.)

(3)  Run main loop while heating with graphite heater core, maintaining plugging branch temperature above that of the main loop.

(4)  Once desired main loop temperature is reached, heaters are adjusted to create a steady-state temperature.

(5)  The plugging flowmeter signal strength is baselined by running the plugging valve from fully open to fully closed and returning to fully open. Finally, a valve position is selected to achieve a desired flow ratio usually achieved by observing the ability to balance heat inputs and outputs.

(6)  Temperature of the plugging flowmeter is regulated carefully to achieve a steady temperature drop, linear with time. Heaters applied downstream of the valve serve to prevent plugging from occurring outside of the plugging valve orifice.

(7)  In order to ensure that oxide precipitation takes place only in the valve orifice, heaters are applied along the balance of the plugging branch plumbing and maximum heat applied. The maximum heating rate is a function of the incoming NaK flow rate combined with the valve cooling rate and is therefore continually adjusted.

(8)  As the temperature falls, the plugging flow meter signal is observed continuously with any major change in trend noted as onset of plugging.

(9)  At the onset of plugging, the dynamic balance of heating and cooling requires less cooling to maintain a linear temperature drop with time. Ultimately, there is a tipping point where the action of plugging drives a reduction in flow rate and therefore decreases the heat input into the plugging valve. At this point, cooling is no longer required and plugging runs until flow stops.

(10)  When flow is reduced to zero, the flowmeter signal hits a floor and conditions are maintained for 5 full minutes.

(11)  Heat is applied to all of the plugging branch and the valve is opened fully to allow hot NaK to flow through. The combination of incoming hot NaK and external heating serves to drive precipitated oxides back into solution, restoring full flow.

Figure 39 plots plugging flowmeter output versus plugging flow temperature during several plugging routines. Step changes in flow signal were attributed to larger solids in the flow stream becoming lodged and/or dislodged in the plugging valve orifice. An approximation of 313 °C (595.4 °F) for onset of plugging is visible in all three traces.
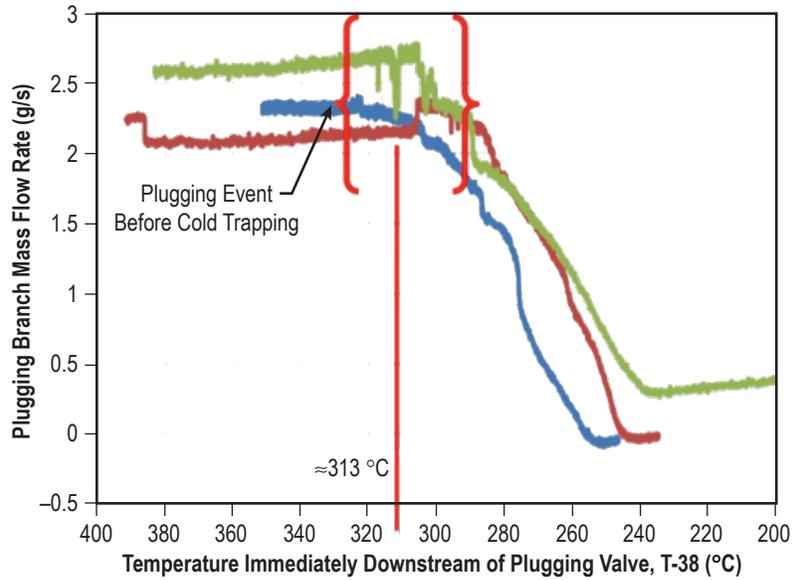
Figure 39.  Prepurification plugging routines.

Figure 40 is a plot of O solubility in NaK with an oxide concentration level highlighted at 313 °C (595.4 °F). This temperature coincides with an oxide saturation concentration of 110 ppm.
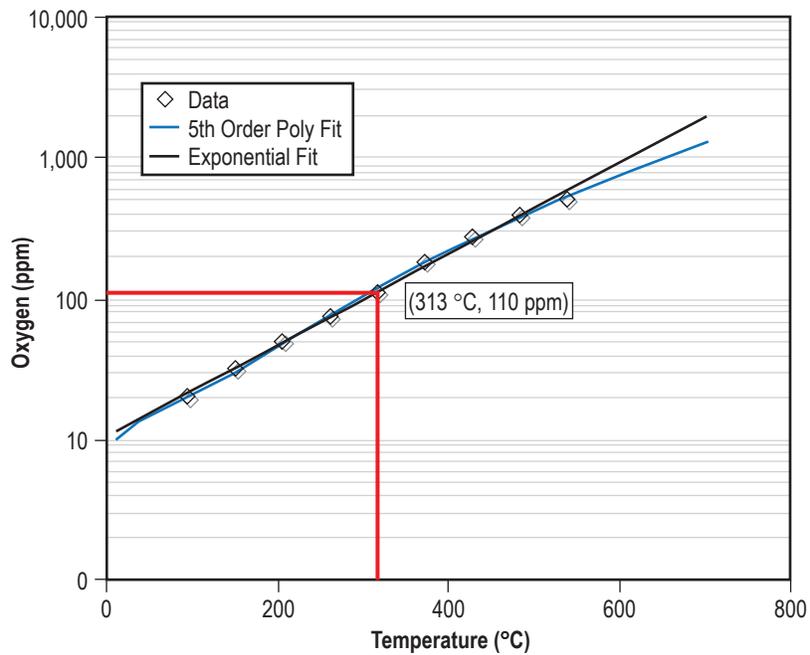


Figure 40.  Resultant contamination measurement based on prepurification plugging routine.

A summary of plugging events is provided in table 6. As shown in table 6, there was a range of flow percentage allowable through the plugging branch in order to achieve a successful plugging event. This represents the system hardware's ability to be adjusted to provide more or less cooling as necessary to achieve steady temperature reduction. In general, the following limitations are identified:

Table 6.  Summary of plugging events.

| Chart | Main Loop Bypass Valve Setting (Turns) | Plugging Valve Setting (Turns) | Main Loop Flow Rate (cc/s) | Main Loop Temperature (°C) | Plugging Branch Flow Rate (cc/s) | Plugging Orifice Temperature (°C) | Plugging Flow to Main Flow Ratio (%) | Plugging Operation Cooling Rate (°C/min) |
|---|---|---|---|---|---|---|---|---|
| *1 | 1 | 2 | 76.0 | 304 | 20.1 | NA (285) | 26.4 | –5.1 |
| *2 | 1 | 3 | 76.7 | 310 | 18.9 | NA (289) | 24.7 | –6.0 |
| *3 | 1.7 | 1.3 | 100.8 | 419 | 18.8 | 306 | 18.7 | –2.5 |
| A | 1.6 | 2.5 | 103.2 | 383 | 10.1 | 323 | 9.8 | –0.9 |
| B | 1.6 | 2.5 | 102.7 | 387 | 10.0 | 304 | 9.8 | –1.2 |
| C | 1.6 | 2.5, 2.4 | 102.1 | 371 | 11.7 | 306 | 11.4 | –1.5 |
| D | 1.6 | 1.4 | 102.1 | 317 | 6.1 | 245 | 6.0 | –3.1 |
| E | 1.6 | 1.4 | 102.8 | 340 | 4.8 | 266 | 4.7 | –1.3 |

*For charts 1 and 2, plugging commenced immediately, indicating that the temperature started too low. Chart 3's plugging flowmeter was not properly calibrated and the chart is not shown in figure 44.

(1)  Higher flow rates and therefore higher plugging branch to main loop flow ratios require greater time to produce a plugging 'event' with the risk of having insufficient cooling at the plugging valve to produce a plugging event.

(2)  Lower flow rates and therefore lower plugging branch to main loop flow ratios cool more rapidly, making identification of precise plugging temperature difficult.

The plugging apparatus may therefore be used quickly to obtain a general idea of contamination level (a range of saturation temperatures) for a system with unknown contaminant content by use of small plugging branch flow rate and high rate of cooling. Following such a plugging event, the plugging apparatus is 'cleaned' by passing heated NaK back through while opening the adjustable orifice (plugging valve) completely. A second plugging operation may then be conducted at a slower rate of cooling close to the temperature range identified above, allowing a more precise identification of saturation temperature.

Figure 41 shows plots for all plugging events using the same flowmeter calibration. Plots A, B, and C are plugging events occurring prior to a purification operation via cold trapping. Plots D and E are plugging events occurring after purification. Note the net reduction in temperature at plugging (major change in slope) between the groups representing the change in NaK saturation temperature.
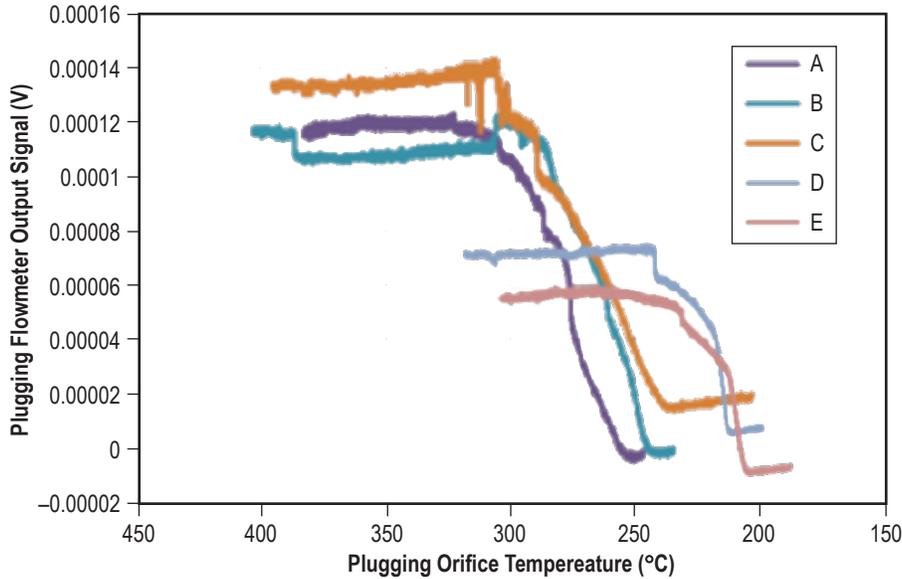
Figure 41. Plots for all plugging events using the same flowmeter calibration.

### 3.2.6 Cold Trapping

A single cold-trapping operation was demonstrated during testing. Given the difficulty and time requirement for running plugging operations, cold trapping was initially postponed until several plugging routines were performed and shown to indicate reasonable repeatability. Figure 42 plots the temperatures of the primary NaK flow loop and the cold trap temperature during a cold-trap routine. Note the temperature delta of 45–70 °C (113–158 °F).

The single cold-trapping operation set out to demonstrate purification by a clear margin, i.e., a clearly visible change in oxide saturation temperature of NaK. Cold trapping took place at two distinct regimes as shown in figure 43 and table 7. Figure 43 plots both pre-cold and post-cold trapping plugging routines for comparison. There is clear indication that the cold-trap routine has changed the parameters of the subsequent plugging routine.

The total mass of NaK loaded into the FTL is ≈3.9 Kg. The trap draws a percentage of total loop volume continuously, purifies it, and then returns it to the main loop. The rate of purification is therefore not linear with time, but will be a maximum at the outset, working towards an O saturation level at the temperature of purification asymptotically. For the purposes of this demonstration, the goal was to demonstrate purification without necessarily quantifying precise rates of decontamination. Figure 44 highlights the oxide saturation level at the temperature measured during the post-purification cold-trapping, successfully indicating a new, lower contaminant concentration of 70 ppm.

38
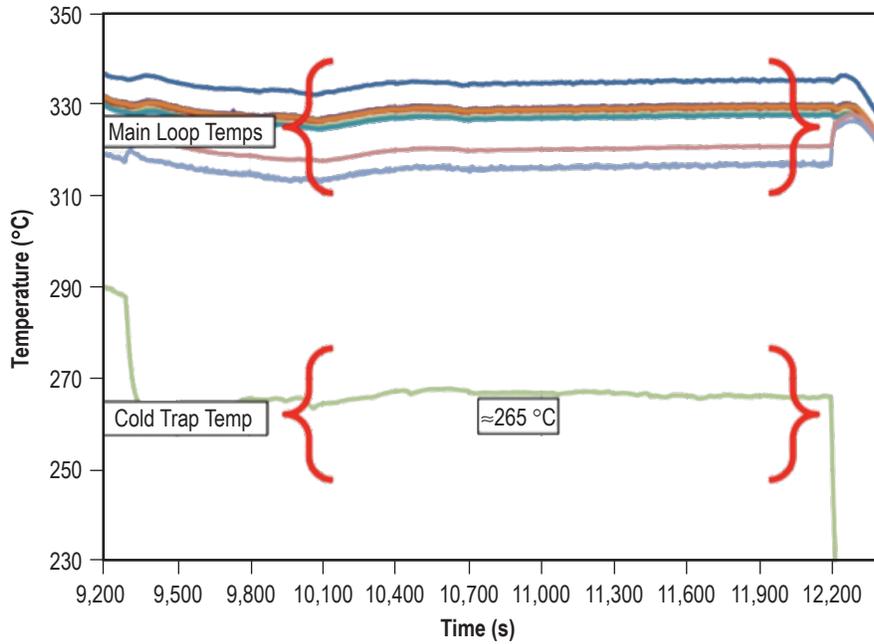
Figure 42.  Purification routine via cold trapping.
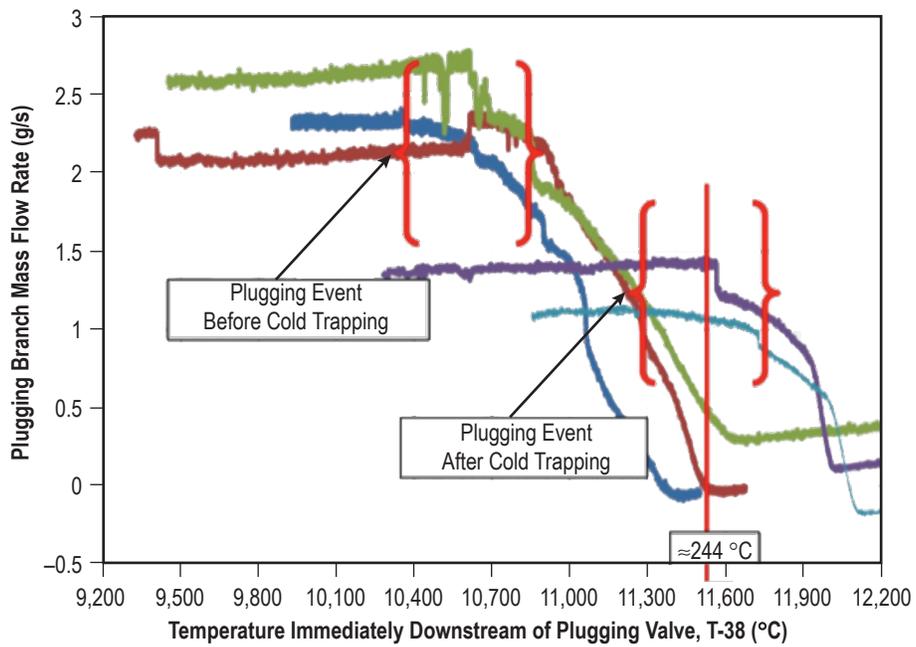


Figure 43.  Postpurification plugging routines compared with prepurification routines.

Table 7. Cold trapping test data.

| Main Loop Temperature (°C) | Main Loop Flow (cc/s) | Cold-Trap Flow* (cc/s) | Cold Trap to Main Loop Flow Ratio (%) | Cold-Trap Temperature (°C) | Duration of Trapping (s) | Total Volume Through Trap (cc) | Total Mass Through Trap (Kg) |
|---|---|---|---|---|---|---|---|
| 334.7 | 115.6 | 13.572 | 13 | 291.6 | 843 | 11,441.2 | 9.1 |
| 328.8 | 111.8 | 9.796 | 10 | 265.8 | 2,790 | 27,330.8 | 21.7 |

*This flow rate is estimated from system models and other flow testing since no flowmeter was installed on the cold trap branch.
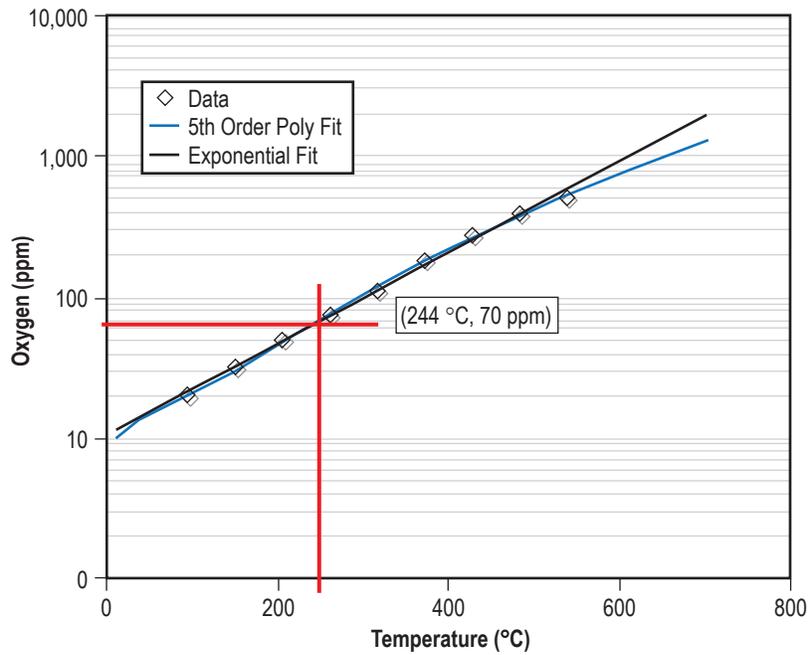


Figure 44. Resultant contamination measurement based on postpurification plugging routine.

# 4. LESSONS LEARNED

Valuable lessons learned during development and testing of the hardware used in this successful testing are documented in this section. While not specifically covered in testing objectives as defined at the outset of this research and development work, these were identified during testing either as 'a-ha' moments or as repeated observations with obvious enabling value for future work.

## 4.1  Flow Measurement

Some mechanism of flow measurement should be provided on all branches of a fluid flow system. Electromagnetic flowmeters are an excellent, noninvasive means of providing a flow measurement provided they are calibrated using a well-known reference. A venturi flowmeter provides a starting reference and subsequently represents a minimal pressure loss to the system.

## 4.2  Electromagnetic Flowmeters

A common observation at the beginning of EM flowmeter operation is the need for high temperature operation to 'wet' the flowmeter, i.e., force the relatively high surface tension NaK to relax and intermingle with its surrounding flow channel. (This can be likened to a drop of water either beading up on a surface (nonwetted) or spreading freely (wetting)). During this testing, it was observed that EM flowmeter signal strength was not subject to this limitation. It is hypothesized that the turbulent flow of the higher flow rates achieved in this current hardware configuration produced a similar result.

## 4.3  Venturi Flowmeter

Venturi flowmeters provide a relatively simple and well-documented method for measuring flow rate in a fluid flow system. The accuracy of a venturi depends wholly on matching the design to the expected flow conditions and ensuring accurate pressure readings are taken.

Careful design of the flow loop and study of the resulting system curve provides the only reliable means for identifying and properly sizing a venturi flowmeter.

Low-pressure drops are usually desired to reduce the overall parasitic losses in a system. The lower the pressure drop allowable, the more difficult to obtain a precise pressure reading. In the case of a venturi flowmeter, a $\Delta P$ PT should be employed. This $\Delta P$ transducer will be very sensitive and should therefore be isolated from any system test and checkout where potentially large pressure transients are expected.

## 4.4 Heat Transfer

Forced convection heat transfer is far more effective than natural convection due to temperature and therefore density changes in a fluid. In fact, natural convection may be identified as a negligible mechanism except when coupled with an appropriate geometry (high vertical aspect ratio such as a vertically oriented reservoir). Initial designs for the heated NaK reservoir employed in the FTL relied on natural convection to mix the NaK flowing through the loop. The final design provided internal flow channels in the flow reservoir to force incoming (cool) NaK to come in direct contact with the graphite heater port in the reservoir, thus allowing maximum absorption of applied heat. This is important to note as heating transients require long durations when heat transfer is not facilitated with effective design, thus forcing much longer testing durations.

It has been repeatedly observed that heat-loss paths are insufficiently estimated, resulting in higher net heating requirements and cooling occurring in critical areas where isothermal behavior is the assumption.

## 4.5 Loop Design Process

Since initial configurations of the FTL were first tested, it has been apparent that there are flow rate/heating/cooling combinations that fall in fairly narrow bands to achieve balanced, steady-state operation for the tubing sizes employed (0.5-in (1.27-cm) and 0.25-in (0.64-cm) nominal tube). Without well-known heat transfer coefficients for natural and forced convection between SS and NaK fluid, effective configurations have been achieved through iterative trial and error.

The trial-and-error process generally began with a preliminary estimate is prepared for expected loop performance. The hardware is then built precisely to carefully match predicted configurations and conditions as much as possible. This configuration is rigorously tested to obtain sufficient data for anchoring the original estimates or identifying areas where estimates are obviously incorrect. Subsequent design work addresses areas where increased design fidelity is required.

## 4.6 Pressure Transducers

Pressure transducers must be carefully selected so that their measurement range will always exceed any exposure they will be subjected to. In the case of fluid flow loops, it is generally a simple process to size a transducer to measure expected pressure drops, which are well known. An additional subtlety of a hermetically-isolated, heated fluid flow loop is the increase in line pressure due to a temperature increase of any blanketing gasses. Care should be taken to combine expected fluid pressures with these changes of gas pressure to arrive at the correct pressure range to be measured.

Care must be taken to calibrate PTs in such a way as to not exceed the measuring range provided by the manufacturers as this range is limited by elastic deformation of a thin metal diaphragm. Exceeding the range will bias future readings and be subject to hysteresis. It is therefore critical that all PTs be specified so that all possible measured pressures fall within the recommended pressure range. It is not recommended to attempt recalibration after testing has commenced as this effectively renders test-to-test comparison of results unusable.

One special case that requires extra attention is the use of $\Delta P$ PTs. The more precise a measurement range, the finer and more fragile the metal diaphragm employed in the transducer and therefore the more susceptible to plastic deformation. It is critical to design calibration and testing procedures to eliminate off-design pressure exposure that effectively render transducers unreliable and unable to produce repeatable results.

## 4.7  Valve Positions

Use of remotely operated valves in a flow system provide excellent flexibility in adjusting areas of study in a flow loop. Some means for recording valve positions in the time-stamped data stream should be provided to allow subsequent correlation. In addition, care should be exercised to ensure that valve positions are repeatable and regularly confirmed by test prior to major testing events.

## 4.8  Thermocouples

For critical temperature measurements, redundancy is essential so that operations may proceed or be safely terminated if a temperature measurement fails. Provide multiple TCs as necessary at critical measuring points.

After identifying critical safety measurements, identify desired measurement locations required for the purposes of studying and carrying out research goals. Only after the above are adequately in place should additional, nonessential measurements be populated.

## 4.9  Fluid System Filtration

A mechanical filter screen is desirable in a heated NaK flow loop. Repeated temperature transients in such a system will transport O from a very distributed initial concentration to discrete deposits of oxides. These deposits may subsequently become suspended in flowing NaK where the rate at which they dissolve back into solution is extremely limited. These discrete particles may become lodged in such a way as to be effective mechanical obstructions. A filter screen located in the loop and subjected to high-velocity, forced fluid flow provides the greatest likelihood that the particles may be dissolved back into solution due to fluid impingement.

## 4.10  Calibration

Calibration should be a distinct part of pretest and checkout only. Once testing commences, any adjustments to signals should be performed by postprocessing on collected data so that all test data has the same baseline. Without this restriction, inter-test comparison of test data is null and void.
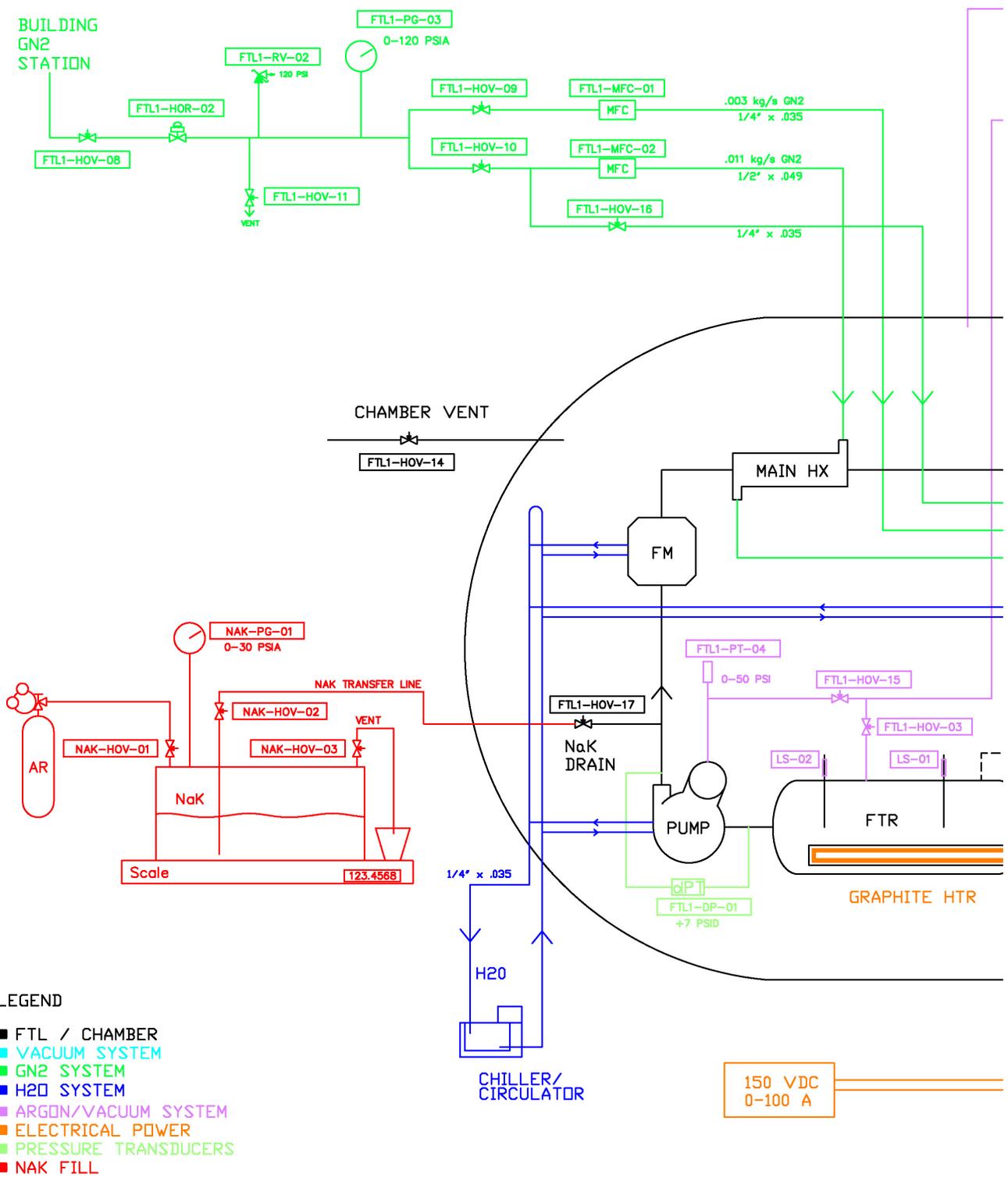
# 5. CONCLUSION

Testing successfully demonstrated flow loop contamination and purification via plugging meter and cold trap. NaK contamination was measured via a plugging meter consisting of a gas-cooled, motor-controlled metering valve and a water-cooled EM flow meter. NaK purification was demonstrated via use of a gas-cooled cold trap with integrated economizer and subsequent contamination measurement via plugging meter as above.

In addition, a nonflight-like mechanical NaK pump provided a robust, high flow rate solution for system testing employing readily available component parts. Full-flow EM flowmeters with unmodified flow channels were shown to have sufficient signal-to-noise ratio to obviate the previous FTL design's need for flow channel modification and subsequent potential flow restriction. A venturi flowmeter was a relatively simple addition to the flow loop and provided calibration reference for EM flowmeters. A reservoir heated via a graphite heater provided effective, rapid NaK heating with a relatively small footprint. Finally, motor-controlled valves provided high-fidelity remote operation during online flow tests.

## APPENDIX A—SYSTEM SCHEMATIC

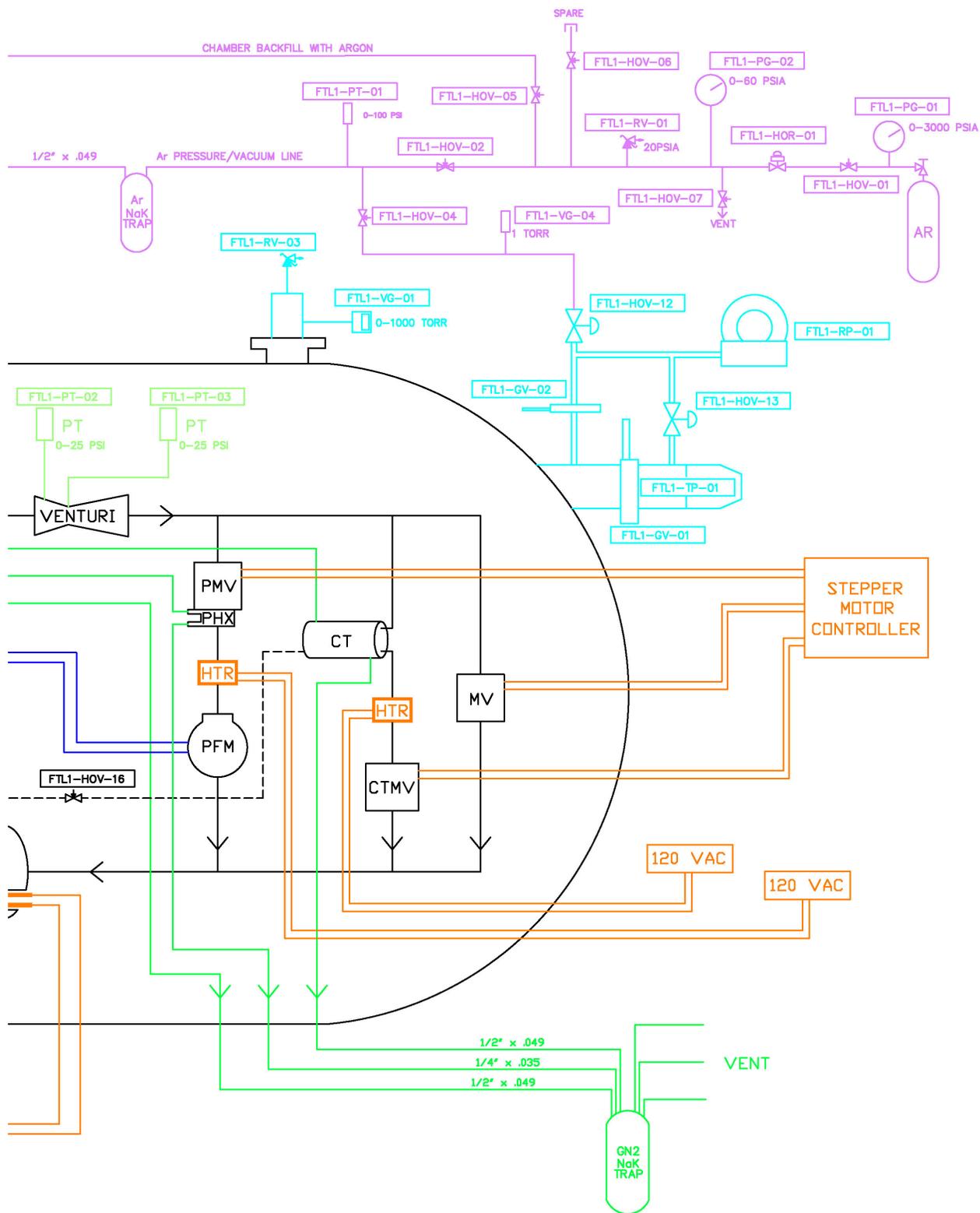Figure 45 shows the system schematic.

BUILDING
GN2
STATION

FTL1-PG-03
0-120 PSIA

FTL1-RV-02
120 PSI

FTL1-HOR-02

FTL1-HOV-08

FTL1-HOV-11
VENT

FTL1-HOV-09

FTL1-MFC-01
MFC

.003 kg/s GN2
1/4" x .035

FTL1-HOV-10

FTL1-MFC-02
MFC

.011 kg/s GN2
1/2" x .049

FTL1-HOV-16

1/4" x .035

CHAMBER VENT

FTL1-HOV-14

MAIN HX

FM

FTL1-PT-04
0-50 PSI

FTL1-HOV-15

NAK-PG-01
0-30 PSIA

NAK TRANSFER LINE

NAK-HOV-02

VENT

NAK-HOV-03

NAK-HOV-01

AR

NaK

Scale          123.4568

FTL1-HOV-17

NaK
DRAIN

FTL1-HOV-03

LS-02          LS-01

FTR

GRAPHITE HTR

PUMP

dPT
FTL1-DP-01
+7 PSID

1/4" x .035

H2O

CHILLER/
CIRCULATOR

150 VDC
0-100 A

LEGEND

■ FTL / CHAMBER
■ VACUUM SYSTEM
■ GN2 SYSTEM
■ H2O SYSTEM
■ ARGON/VACUUM SYSTEM
■ ELECTRICAL POWER
■ PRESSURE TRANSDUCERS
■ NAK FILL

46

Figure 45.  System schematic.

# APPENDIX B—MP PUMP PERFORMANCE CURVE

The MP Pump performance curve is shown in figure 46.

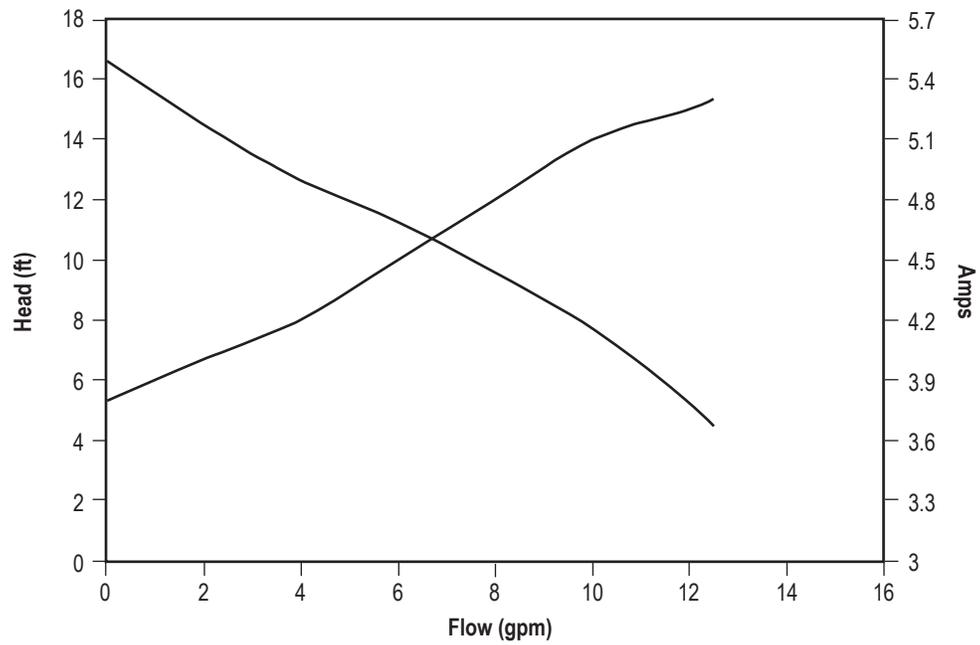Figure 46.  MP Pump performance curve.

# APPENDIX C—THERMOCOUPLE LOCATIONS

Table 8 shows the 36 TC locations.

Table 8.  Thermocouple locations.

| No. | Description |
|---|---|
| T-01 | $\Delta P$ PT, DP-01 |
| T-02 | Absolute PT, PT-01, venturi upstream |
| T-03 | Absolute PT, PT-02, venturi throat |
| T-04 | Absolute PT, PT-04, NaK pump Ar blanket |
| T-05 | NaK temperature via thermal well, immediately downstream of reservoir |
| T-06 | NaK temperature via thermal well, immediately downstream of main EM flowmeter |
| T-07 | NaK temperature via thermal well, immediately downstream of main $GN_2$ HX |
| T-08 | NaK temperature via clamped on TC, immediately upstream of venturi |
| T-09 | NaK temperature via thermal well, at plugging branch tee |
| T-10 | NaK temperature via clamped-on TC, immediately upstream of bypass valve |
| T-11 | NaK temperature via clamped-on TC, main loop between cold trap and plugging branch exit tees |
| T-12 | NaK temperature via thermal well, immediately upstream of reservoir |
| T-13 | Water temperature, mechanical pump cooling inlet |
| T-14 | Water temperature, mechanical pump cooling outlet |
| T-15 | Water temperature, main EM flowmeter inlet |
| T-16 | Water temperature, main EM flowmeter outlet |
| T-17 | Water temperature, plugging EM flowmeter inlet |
| T-18 | Water temperature, plugging EM flowmeter outlet |
| T-19 | $GN_2$ temperature, main HX inlet |
| T-20 | $GN_2$ temperature, main HX outlet |
| T-21 | $GN_2$ temperature, plugging HX inlet |
| T-22 | $GN_2$ temperature, plugging HX outlet |
| T-23 | $GN_2$ temperature, cold trap inlet |
| T-24 | $GN_2$ temperature, cold trap outlet |
| T-25 | NaK temperature via clamped-on TC, immediately downstream of plugging valve |
| T-26 | NaK temperature via thermal well, downstream of plugging valve, upstream of plugging branch heater |
| T-27 | NaK temperature via thermal well, downstream of plugging branch heater and plugging EM flowmeter |
| T-28 | NaK temperature via clamped-on TC, cold trap inlet |
| T-29 | NaK temperature via thermal well, coolest region of cold trap |
| T-30 | NaK temperature via clamped-on TC, cold trap outlet |
| T-31 | Cartridge heater core temperature, plugging branch heater |
| T-32 | Cartridge heater core temperature, cold trap branch heater |
| T-33 | SS reservoir temperature at graphite heater port |
| T-34 | Ar blanket temperature at mechanical pump |
| T-35 | SS pump body temperature |
| T-36 | SS reservoir temperature at outer wall |

# REFERENCES

1. Nainiger, J.: "Affordable Fission Surface Power System Study Final Report," NASA Exploration Systems Mission Directorate Report, October 2007.

2. Mason, L.S.: "A Comparison of Fission Power System Options for Lunar and Mars Surface Applications," *NASA/TM—2006–214120*, Glenn Research Center, Cleveland, OH, February 2006.

3. Mason, L.S.: "A Practical Approach to Starting Fission Surface Power Development," *NASA/TM—2006–214366*, Glenn Research Center, Cleveland, OH, July 2006.

4. Mason, L.S.; Poston, D.; and Qualls, L.: "System Concepts for Affordable Fission Surface Power," *NASA/TM—2008–215166*, Glenn Research Center, Cleveland, OH, January 2008.

5. Palac, D.; Mason, L.; and Harlow, S.: "Fission Surface Power Technology Development Status," *NASA/TM—2009–215602*, Glenn Research Center, Cleveland, OH, March 2009.

6. Mausteller, J.W.; Tepper, F.; and Rodgers, S.J.: *Alkali Metal Handling and Systems Operating Techniques*, Gordon and Breach, New York, 1967.

7. Garber, A.E.; Webster, K.L.; Godfroy, T.J; et al.: "Interim Report: Performance Testing of a 7-Pin Bundle in the Fission Surface Power—Primary Test Circuit," Marshall Space Flight Center, Huntsville, AL, July 2010.

8. Godfroy, T.J.; Bradley, D.E.; Pearson, J.B.; et al.: "Hardware-Based Assessment of Subscale Sodium-Potassium Cooled Fission Power Reactor Simuators and Related Component Designs," *NASA/TP—2011–xxxxx*, Marshall Space Flight Center, Huntsville, AL, June 2011.

9. Stepanoff, A.J.: *Centrifugal and Axial Flow Pumps: Theory, Design, and Application*, Wiley, New York, 1957.

# REPORT DOCUMENTATION PAGE

| 1. REPORT DATE *(DD-MM-YYYY)* | 2. REPORT TYPE | 3. DATES COVERED *(From - To)* |
|---|---|---|
| 01–10–2011 | Technical Publication | |

**4. TITLE AND SUBTITLE**

Online Oxide Contamination Measurement and Purification Demonstration

5a. CONTRACT NUMBER

5b. GRANT NUMBER

5c. PROGRAM ELEMENT NUMBER

**6. AUTHOR(S)**

D.E. Bradley,* T.J. Godfroy,** K.L. Webster, A.E. Garber, K.A. Polzin, and D.J. Childers

5d. PROJECT NUMBER

5e. TASK NUMBER

5f. WORK UNIT NUMBER

**7. PERFORMING ORGANIZATION NAME(S) AND ADDRESS(ES)**

George C. Marshall Space Flight Center
Huntsville, AL  35812

**8. PERFORMING ORGANIZATION REPORT NUMBER**

M–1322

**9. SPONSORING/MONITORING AGENCY NAME(S) AND ADDRESS(ES)**

National Aeronautics and Space Administration
Washington, DC  20546–0001

**10. SPONSORING/MONITOR'S ACRONYM(S)**

NASA

**11. SPONSORING/MONITORING REPORT NUMBER**

NASA/TP—2011–216473

**12. DISTRIBUTION/AVAILABILITY STATEMENT**

Unclassified-Unlimited
Subject Category 20
Availability: NASA CASI  (443–757–5802)

**13. SUPPLEMENTARY NOTES**

Prepared by the Propulsion Systems Department, Engineering Directorate
*Yetispace, Inc., Huntsville, AL   **Maximum Technology Corporation, Huntsville, AL

**14. ABSTRACT**

Liquid metal sodium-potassium (NaK) has advantageous thermodynamic properties indicating its use as a fission reactor coolant for a surface (lunar, martian) power system. A major area of concern for fission reactor cooling sysgtems is system corrosion due to oxygen contaminants at the high operating temperatures experienced. A small-scale, ≈4-L capacity, simulated fission reactor cooling system employing NaK as a coolant was fabricated and tested with the goal of demonstrating a noninvasive oxygen detection and purification system. In order to generate prototypical conditions in the simulated cooling system, several system components were designed, fabricated, and tested. These major components were a fully-sealed, magnetically-coupled mechanical NaK pump, a graphite element heated reservoir, a plugging indicator system, and a cold trap. All system components were successfully demonstrated at a maximum system flow rate of ≈150 cc/s at temperatures up to 550 ºC. Coolant purification was accomplished using a cold trap before and after plugging operations which showed a relative reduction in oxygen content.

**15. SUBJECT TERMS**

NaK, mechanical NaK pump, electromagnetic flowmeter, NaK plugging meter, NaK cold trap, online oxygen measurement in NaK, hardware, test

| 16. SECURITY CLASSIFICATION OF: | | | 17. LIMITATION OF ABSTRACT | 18. NUMBER OF PAGES | 19a. NAME OF RESPONSIBLE PERSON |
|---|---|---|---|---|---|
| a. REPORT | b. ABSTRACT | c. THIS PAGE | | | STI Help Desk at email: help@sti.nasa.gov |
| U | U | U | UU | 62 | 19b. TELEPHONE NUMBER *(Include area code)* STI Help Desk at: 443–757–5802 |